LABORATORI NAZIONALI DI FRASCATI
SIS-Pubblicazioni
LNF-98/039(P)
17 Novembre 1998

The DEAR case

(The DEAR Collaboration)

S. Bianco[a], A.M. Bragadireanu[a,f], F.L. Fabbri[a], C. Guaraldo[a], M. Iliescu[a,f], T.M. Ito[a,m], V. Lucherini[a], C. Petrascu [a,f], M. Bregant[b], E. Milotti[b], A. Vacchi[b], E. Zavattini[b], M. Augsburger[c], D. Chatellard[c], P. Knowles[c], F. Mulhauser[c], L.A. Schaller[c], L. Schellenberg[c], H. Schneuwly[c], J.-P. Egger[d], D. Varidel[d], W.H. Breunlich[e], M. Cargnelli[e], B. Gartner[e], R. King[e], B. Lauss[e], J. Marton[e], J. Zmeskal[e], T. Ponta[f], S.N. Nakamura[g], T. Koike[h], R.S. Hayano [i], M. Hori[i], T. Ishikawa[i], T. Ishiwatari[j], M. Iwasaki[j], Y. Akaishi[k], G. Beer[l], A.C. Sanderson[l], R. Seki[m,n]

[a] *INFN - Laboratori Nazionali di Frascati, C.P. 13, Via E. Fermi 40, I-00044 Frascati , Italy*
[b] *Univ. degli Studi di Trieste, Dip. di Fisica and INFN Sezione di Trieste, Via A. Valerio 2, I-34127, Trieste, Italy*
[c] *Univ. de Fribourg, Inst. de Physique, Bd. de Perolles, CH-1700 Fribourg, Switzerland*
[d] *Univ. de Neuchâtel, Inst. de Physique, 1 rue A.-L. Breguet, CH-2000 Neuchâtel, Switzerland*
[e] *Institute for Medium Energy Physics, Austrian Academy of Sciences, Boltzmanngasse 3, A-1090 Vienna, Austria*
[f] *Inst. of Physics and Nuclear Engineering "Horia Hulubei", Dept. of High Energy Physics, P.O. Box MG-6 R-76900 Magurele, Bucharest, Romania*
[g] *Inst. of Physical and Chemical Research (RIKEN), 2-1 Hirosawa, Wako, Saitama 351-01, Japan*
[h] *Hokkaido Univ., Dept. of Physics, N8W5 Kikta, Sapporo 060, Japan*
[i] *Univ. of Tokyo, Dept. of Physics, 7-3-1 Hongo, Bunkyo, Tokyo 113, Japan*
[j] *Tokyo Institute of Technology 2-12-1 Ookayama Meguro, Tokyo 152, Japan*
[k] *KEK, High Energy Accelerator Research Organization, Tanashi Campus 3-2-1 Midori Tanashi, Tokyo 188, Japan*
[l] *Univ. of Victoria, Dept. of Physics and Astronomy, P.O. Box 3055 Victoria, B.C. V8W 3P6, Canada*
[m] *W.K. Kellogg Radiation Laboratory, California Institute of Technology Pasadena, California 91125*
[n] *Department of Physics and Astrophysics, California State University, Northridge, CA 91330*

PACS: 13.75.Jz, 36.10.-k

Submitted to Physics Report

Abstract

The scientific program and the experimental setup of the DEAR (DAΦNE Exotic Atom Research) experiment at the new ϕ-factory DAΦNE of Laboratori Nazionali di Frascati, are described. The objective of DEAR is to perform a 1% measurement of the K_α line shift due to the strong interaction in kaonic hydrogen. A measurement will also be performed on kaonic deuterium for the first time. The aim is to investigate low-energy $\bar{K}N$ physics and to understand SU(3) chiral symmetry breaking. The setup takes advantage of the unique features of the "kaon beam" from the ϕ decay in DAΦNE; of a low-temperature pressurized gaseous target; and of a detector for soft X rays – the Charge-Coupled Device (CCD) – characterized by a good resolution and by an unprecedented background rejection capability. The DEAR experiment represents a major effort in the study of low energy $\bar{K}N$ interactions and has the potential to produce a breakthrough in the field.

Contents

1 Introduction

The low energy kaon-nucleon interaction is still a largely unexplored field experimentally. More than 15 years ago, R.H. Dalitz made the following statement [1]:

> The most important experiment to be carried out in low energy K-meson physics today is the definitive determination of the energy level shift in the K^-p and K^-d atoms, because of their direct connection with the physics of the $\bar{K}N$ interaction and their complete independence from all other kinds of measurements which bear on this interaction.

This statement can be repeated today. Moreover, the lack of experimental results has had a negative impact on theoretical developments: in addition to the poorly determined low-energy parameters, the KN sigma term - a vital non-perturbative QCD quantity - has remained virtually undetermined. This has created a serious disparity within the recent theoretical efforts based on QCD chiral effective Lagrangians.

This paper describes DEAR (DAΦNE Exotic Atom Research)– one of the first experiments collecting data at the new ϕ-factory DAΦNE of Laboratori Nazionali di Frascati dell'INFN. DEAR will observe X rays from kaonic hydrogen and kaonic deuterium, using the "K^- beam" from the decay of ϕs produced by DAΦNE, a cryogenic pressurized gaseous target and Charge-Coupled Devices (CCDs) as X-ray detectors. The experiment represents the most powerful effort yet launched in the study of kaon-nucleon physics. This is due to:

- the low momentum, monochromatic, high purity and intense kaon beam from DAΦNE with respect to kaon beams used in similar experiments;

- the resolution and, above all, background rejection capability of CCDs, which makes them *the detectors* for soft X-ray measurements in accelerator backgrounds, as has been demonstrated recently by the results obtained with CCDs in exotic atom experiments at PSI (Villigen) and at LEAR (CERN);

- the use of a moderate-density target to reduce the Stark mixing which causes strong absorption of the kaon from high-*n* atomic states. This will allow us to obtain a high-statistics X-ray data sample. The number of events collected by DEAR in *one week* with kaonic hydrogen at 10^{32}cm^{-2}s^{-1} luminosity will surpass by an order of magnitude the current world data set.

The objective of DEAR is the precise determination of the isospin dependent $\bar{K}N$ scattering lengths, through a 1% measurement of the K_α line shift in kaonic hydrogen.

The first measurement on kaonic deuterium will also be performed. Thus a breakthrough in the field of low-energy $\bar{K}N$ interactions appears realistic with DEAR.

A measurement of the K_α line shift to 1% will yield the isospin-dependent $\bar{K}N$ scattering lengths with a precision of a few percent. This will drastically change the present status of the low energy $\bar{K}N$ phenomenology, and also provide a clear assessment of the SU(3) chiral effective Lagrangian approach to low energy hadron interactions. An improved determination of the KN sigma terms, quantities which give the degree of chiral symmetry breaking, then becomes possible. The KN sigma terms are also a very sensitive probe of the strangeness content of the nucleon, even more so than the πN sigma term.

The paper is organized as follows: Section 2 reviews the scientific case and Section 3 describes the principle of the measurement and the experimental setup. In Section 4 the main features of the Charge-Coupled-Device detector are described. The multi-faceted problem of the machine background is treated in Section 5. The simulation of X-ray event rate and CCD background from the electromagnetic and hadronic cascades originating from particles coming from the machine and kaon beam is reported in Section 6. Error estimates, a crucial item for a precision measurement, are discussed in Section 7, followed by conclusions and perspectives in Section 8.

References

[1] R.H. Dalitz *et al.*, Proceedings of the *Conference on Hypernuclear and Kaon Physics*, ed. by B. Povh, Max–Plank Institute Report MPI H–1982–V20 (MPI, Heidelberg 1982), p. 201.

2 The DEAR scientific case

2.1 The low-energy kaon-nucleon interaction

The $\overline{K}N$ interaction at low energies is neither simple nor well understood.

The K^-p interaction can occur through both I=0 and I=1 isospin states and there are several open inelastic channels at threshold (1432 MeV, total energy in the center of mass). The K^-p channel is coupled by charge exchange to $\overline{K}^0 n$ and, furthermore, is strongly coupled to several πY channels (where $Y = \Lambda,\ \Sigma$):

$$K^-p \to K^-p \tag{1}$$

$$K^-p \to \overline{K}^0 n\ -5\,\mathrm{MeV} \tag{2}$$

$$K^-p \to \pi\Sigma\ +100\,\mathrm{MeV} \tag{3}$$

$$K^-p \to \pi^0\Lambda\ +180\,\mathrm{MeV} \tag{4}$$

Moreover, this energy region is dominated by the presence of the s-wave subthreshold $\Lambda\,(1405)$ resonance with strangeness -1, $I = 0$, which decays into $\pi\Sigma$ with a branching ratio of 100% and whose nature is still an open problem. Other resonances occur in different partial waves, both above threshold (the Λ(1520) in d-wave) and below threshold (the Σ(1385) in p-wave).

Experimentally, the low-energy $\overline{K}N$ interaction has been investigated through (1) low energy K^-p scattering experiments, (2) branching ratio measurement of kaon absorption at rest in hydrogen bubble chambers, and (3) measurement of kaonic hydrogen atom X rays. In addition, $\Sigma\pi$ invariant mass spectra below the $\overline{K}N$ threshold have been used in the theoretical analysis of the low energy $\overline{K}N$ system. The kaonic hydrogen X-ray measurement is important in that it gives information in the energy range between that accessible with the scattering experiment and that accessible with the $\Sigma\pi$ invariant mass spectra.

2.2 Exotic atoms

By exotic atom, one means any system in which a negatively-charged particle other than an electron - a muon (μ^-), or hadrons like a pion (π^-), a kaon (K^-), an antiproton ($\bar{p}$), or a sigma hyperon (Σ^-) - orbits a nucleus, under conditions in which the principal interaction with the nucleus is electromagnetic. In the case of hadronic atoms, after the deexcitation

processes, when the hadron has reached one of the lowest levels, it interacts strongly with the nucleus.

2.2.1 Kaonic hydrogen

The formation mechanism of a kaonic hydrogen atom is as follows: a negative kaon enters a hydrogen target and loses kinetic energy by ionization and excitation of the hydrogen molecules until it is captured in an atomic orbit around the proton (replacing the electron). It is generally accepted that the capture orbit has the principal quantum number $n_{capt} \simeq \sqrt{\mu/m_e} \simeq 25$ (μ and m_e are, respectively, the reduced mass of the K^-p system and the electron mass), i.e., it is a highly excited level – the radius of the kaonic system corresponding to that of the hydrogen K-shell electrons. Then, the kaon cascades down through the series of atomic states.

Three processes compete in the deexcitation of kaonic hydrogen: dissociation of the surrounding molecules, external Auger transitions and radiative transitions. At high density, as in liquid hydrogen, Stark mixing also becomes relevant. The strong electric field of protons in collisions with neighbouring nuclei causes a mixing between degenerate states with the same principal quantum number and different angular momenta - the consequence being nuclear absorption from high-n states, preventing the kaon from reaching low-lying states via emission of K- and L- series X rays. Under normal experimental conditions in hydrogen, the cascade is much faster and not affected by the kaon lifetime.

When the kaon reaches a low-n state with a small angular momentum, it is absorbed by the proton due to the strong interaction. The strong interaction causes a shift of the low-lying levels from their pure electromagnetic positions, and the widths are increased. However, the effects are appreciable only in the $1s$ state (only for the K-series lines). In practice, since the energy spacings between adjacent lines of the $K_{\geq\beta}$ complex are much smaller than the detector energy resolution and the expected $1s$ width, the K_α (6.5 keV) line is most important in determining the level shift and the width of the $1s$ level.

The shift ϵ and the width Γ of the 1*s* state of kaonic hydrogen are related in a fairly model-independent way to the real and imaginary part of the *s*-wave scattering length a_{K^-p}, which is a complex quantity, due to the strong inelasticity represented by the coupling to several channels open at threshold:

$$\epsilon + \frac{i}{2}\Gamma = 2\alpha^3\mu^2 a_{K^-p} = (412\,\mathrm{eVfm}^{-1}) \cdot a_{K^-p} \tag{5}$$

with μ the reduced mass and α the fine structure constant. This expression is known as the *Deser-Trueman formula* [1].

2.3 Experiments on kaonic hydrogen

Three measurements of kaonic hydrogen X rays were carried out at CERN and the Rutherford Laboratory in the late 70's through the early 80's [2,3,4]. Recently, a fourth measurement has been performed at KEK [5].

In the three old measurements, a liquid hydrogen target and Si(Li) detectors were used. Davies $et\ al.$ [2] observed a peak at 6.52$\pm$0.06 keV, which they attributed to the K_α line. Izycki *et al.* [3] observed a weak pattern of 3 lines at 6.96$\pm$0.09, 7.99$\pm$0.07 and 8.64$\pm$0.10 keV, respectively, which they assigned to the K_α, K_β and K_γ lines. Bird *et al.* [4] identified a similar series of three lines.

All three spectra suffered from large background and low statistics: X-ray signals were very difficult to identify, having been strongly attenuated by the Stark effect in liquid hydrogen. A common feature, despite the low quality of the data, was that the sign of the shift and, consequently, that of the real part of the K^-p scattering length, was *positive* which implied an *attractive* strong interaction. This was in striking contradiction to the results of the analyses of the other low-energy data (K^-p cross sections for elastic and inelastic processes, branching ratios for K^-p absorption at rest, $\pi\Sigma$ invariant mass distribution), extrapolated to threshold and below, which showed a *negative* real part of the scattering length and therefore a *repulsive* strong interaction.

This discrepancy between X-ray measurements and the other low-energy data is often referred to as the *"kaonic hydrogen puzzle"*. This "puzzle" has received considerable theoretical attention with about 15 years of effort to reconcile the two sets of data. However, no satisfactory theoretical explanation was found and the various attempts to find a scattering parameter set for a phenomenological potential which fitted the other low-energy data together with kaonic hydrogen measurements, were unsuccessful. Recently, a fourth measurement has been performed at KEK which, for the first time, reported a convincing X-ray spectrum [5]. In addition, this measurement reported a negative energy shift, which is consistent with the analyses of the other low-energy data. It is now clear, after the KEK results [5], that nothing had to be reconciled — the so-called "puzzle" was created by the poor quality of the data.

2.3.1 The KpX experiment at KEK

The recently reported *KpX* experiment (KEK-PS E228) [5] succeeded, for the first time, in observing a distinct K_α X-ray peak in kaonic hydrogen transitions. Experimental difficulties with which the three previous experiments had to deal were overcome by some novel techniques — the use of a gaseous hydrogen target and a two-pion tagging method, both of which turned out to be very effective in improving the signal-to-noise ratio.

The experiment was performed at the KEK 12 GeV Proton Synchrotron. Negative kaons of 600 MeV/c from the K3 beam line were slowed in a carbon degrader and brought to rest in the gaseous hydrogen target. A low-temperature pressurized gaseous hydrogen target (100 K, 4 atm) was chosen as a compromise between the kaon stopping rate and the loss of X-ray yield due to Stark mixing. X rays from kaonic hydrogen were detected by as many as sixty Si(Li) X-ray detectors, placed directly inside the target chamber.

High energy γ rays produced by K^-p absorption reactions, directly from π^0s, or as decay products of Λ and Σ^+ decay, were the major source of background in the previous measurements. There are, however, branches with a yield of $\sim 50\%$ which are free from γ rays: they are reactions of the type $K^-p \rightarrow \Sigma^{\pm}\pi^{\mp}$ followed by $\Sigma^{\pm} \rightarrow n\pi^{\pm}$, which are characterized by the presence of two charged pions having momenta higher than 150 MeV/c in the final state. It was thus possible to exclude all reactions producing high energy γ rays by tagging on two charged pions with momenta higher than 150 MeV/c. Moreover, since the lifetime of the charged Σ particle is short, the K^-p reaction and the Σ decay could be regarded as taking place approximately at the same point. The requirement that the two-pion vertex occur in the hydrogen volume, with an appropriate time of flight, allowed one to select only kaons stopping in hydrogen.

The overall statistics were insufficient to perform a precision measurement. However, the result:

$$\varepsilon = -327 \pm 63(stat.) \pm 11(syst.)\ \mathrm{eV} \tag{6}$$

$$\Gamma_{1s} = 407 \pm 208(stat.) \pm 100(syst.)\ \mathrm{eV} \tag{7}$$

solves the long-standing "kaonic hydrogen puzzle". These new results are in agreement with the analyses of the other low-energy data and in contradiction to the previous X-ray measurements. The $1s$ level shift turns out to be negative, and consequently, the real part of the scattering length is also negative, indicating that the kaon-proton atomic system is less bound due to the strong interaction.

2.4 The $\bar{K}N$ scattering lengths

The strangeness of $\bar{K}$ is -1 and the isospin is $1/2$, with $I_3 = (1/2, -1/2)$ for $(\bar{K^0}, K^-)$. With the nucleon isospin assignment of $1/2$, $I_3 = (1/2, -1/2)$ for (p, n), the $\bar{K}N$ scattering lengths, a_{K^-N}, are expressed in terms of the scattering lengths in the specific (s-channel) isospin states:

$$a_{K^-p} \quad = \quad \frac{1}{2}(a_0 + a_1) \tag{8}$$

$$a_{K^-n} \;=\; a_1\,, \tag{9}$$

where a_0 and a_1 are the scattering lengths in the isospin $I = 0$ and 1 states, respectively. The $\bar{K}^0 p$ and $\bar{K}^0 n$ scattering lengths are expressed in a similar way,

$$a_{\bar{K}^0 p} \;=\; a_1 \tag{10}$$

$$a_{\bar{K}^0 n} \;=\; \frac{1}{2}(a_0 + a_1)\,. \tag{11}$$

Here, we assume the strong interaction to preserve the isospin invariance by ignoring small mass differences in each isospin group. The mass differences generate the 0.05% difference of the reduced masses of the K^-n and K^-p systems and the 0.5% in the reduced masses of the K^-N and $\bar{K}^0 N$ systems. The mass differences affect the scattering lengths by shifting the center-of-mass of the systems. Their major effect appears in the kinematical factor of the scattering length as in Eq. (14) below. We ignore the effect in discussions here, since it is less than 1 % . Note that, in practice, the effect is included in the actual three-body calculations of the K^-d scattering length that we will discuss below.

The terms a_0 and a_1 are the key parameters describing the $\bar{K}N$ interaction at threshold. In the DEAR experiment, we will determine a_0 and a_1 from the $1s$ shifts and widths in the kaonic hydrogen and deuterium atoms. These shifts and widths due to the strong interaction are proportional to the K^-p and K^-d scattering lengths,

$$\epsilon + \frac{i}{2}\Gamma \;=\; (412\,\mathrm{eVfm}^{-1}) \cdot a_{K^-p}, \tag{12}$$

$$\epsilon + \frac{i}{2}\Gamma \;=\; (601\,\mathrm{eVfm}^{-1}) \cdot a_{K^-d}. \tag{13}$$

These simple relations are known to hold quite accurately for these atoms [6], their corrections being smaller than 1 %. The higher-order corrections tend to cancel between the two sides of each expression, and the Coulomb correction is quite small in these charge-one systems. We can thus safely consider these relations to be exact and regard the precision of the shift and width measurements to be that of the scattering lengths a_{K^-p} and a_{K^-d}.

The term a_{K^-d} is related to a_0 and a_1 in the following way:

$$a_{K^-d} = 2\left(\frac{m_N + m_K}{m_N + m_K/2}\right) a^{(0)} + C, \tag{14}$$

where

$$a^{(0)} = \frac{1}{2}(a_{K^-p} + a_{K^-n}) = \frac{1}{4}(3a_1 + a_0) \tag{15}$$

corresponds to the (t-channel) isoscalar $\bar{K}N$ scattering length. The first term in Eq. (14) represents the lowest-order impulse approximation – K^- scattering from each (free) nucleon. The second term, C, includes all higher-order contributions, representing all other

physics associated with the $\bar{K}d$ three-body interaction. Note that the kinematic factor in the parentheses of Eq. (14), which equals 1.21, is due to the shift in the center of mass from the $\bar{K}N$ system to the $\bar{K}d$ system. Numerically, C is not negligible and, in fact, is larger than the first term, as we will see in the following subsection. The extraction of a_{K^-n} from a_{K^-d} thus requires a more complicated analysis than the impulse approximation.

2.4.1 Determination of the $\bar{K}N$ scattering lengths

It is well known that a three-body problem is solvable by the use of Faddeev equations when the two-body interactions among them are specified. The π^-d system is one three-body problem that has been investigated extensively [7]. The theoretical treatments [8,9,10] provide information on the π^-n interaction from that of the π^-d and π^-p interaction, thereby yielding the π^-n and (t-channel) isoscalar πN scattering lengths. Such extraction involves the technical complication caused by a large cancellation of the π^-p and π^-n scattering lengths. This cancellation is not a mere accident; the two scattering lengths vanish in the chiral limit in which the pion mass vanishes. In spite of the complication, the π^-n scattering length has been extracted successfully.

The K^-d three-body problem includes the further complication that the K^-p and K^-n interactions involve significant inelastic interactions, as shown in Eqs. (2)-(4). The K^-p and K^-n scattering lengths are thus complex with large magnitudes of the imaginary parts, and so is the K^-d scattering length. Incorporating $\bar{K}N$ scattering data and its sub-threshold behavior, the two-body potentials are determined in a coupled-channel formalism including both elastic and inelastic channels. Three-body Faddeev equations are then solved by the use of the potentials, taking account of coupling among the multi-channeled interactions.

Table 1 shows the results of the K^-d three-body calculations [8, 9, 10]. These calculations used the $\bar{K}N$ potentials constructed to produce the low-energy $\bar{K}N$ data. Each calculation used a somewhat different potential, which was considered to be the best at the time of the calculation. For simplicity, in the upper part of Table 1, we show $a_0, a_1 (= a_{K^-n})$, and a_{K^-p} scattering lengths that are compatible with the $\bar{K}N$ potentials used in each calculation. The variations among their values indicate the differences among the $\bar{K}N$ potentials used in these calculations. In the lower part of Table 1, the values of the column $a^{(0)} = \frac{1}{2}(a_{K^-p} + a_{K^-n})$ indicate the input to each calculation, and the scattering length column a_{K^-d} lists the result of each three-body calculation.

Before proceeding, we note that the magnitude of the real part of $2a^{(0)}$ is far smaller than that of a_{K^-d}, as in the case of the pion, while the imaginary parts are of similar

magnitudes.

The DEAR results for the K^-p and K^-d atomic shifts and widths, hence a_{K^-p} and a_{K^-d}, are analyzed using three-body calculations to yield a_0 and a_1. If a 1% determination of the shifts and widths is achieved, how precisely are a_0 and a_1 determined? This is a somewhat complicated question, but we estimate the resulting precision of a_0 and a_1 as follows.

The three-body calculations quoted above used the same Faddeev equation although the detailed treatments differed somewhat. We expect the Faddeev equation to be used also in analyses of the DEAR data. Accordingly, we view Table 1 as a list of three calculations to extract a_0 and a_1 from different values of a_{K^-p} and a_{K^-d}. That is, Table 1 is now viewed as a list of the a_0 and a_1 that are determined from "the experimental values" of a_{K^-p} and a_{K^-d}.

Following this procedure, we find that a 1% precision of a_{K^-p} and a_{K^-d} would determine a_0 and a_1 with a precision of

$$\delta a_0 = 1\,\%, \tag{16}$$

$$\delta a_1 = 3\,\%. \tag{17}$$

In this estimate, we have combined the results of the three different calculations. The estimate thus includes consequences of possible systematic errors in the theoretical calculations. That is, if we were to perform a specific calculation using a_{K^-p} and a_{K^-d} with a 1% uncertainty, the uncertainty of a_0 and a_1 would be even smaller. Note that among the above scattering lengths, a_{K^-p} is the quantity that enters in the phenomenological determination of the KN sigma term in the most frequently used formulation using the $K^\pm p$ system. When the $K^\pm n$ system is used, it is $a_{K^-n} = a_1$.

Table 1: Multi-channel $\bar{K}d$ scattering length calculations

Ref.	a_0	$a_1 = a_{K^-n}$	a_{K^-p}
[8]	$-1.77 + i0.73$ fm	$0.41 + i0.54$ fm	$-0.68 + i0.64$ fm
[9]	$-1.69 + i0.76$ fm	$0.28 + i0.67$ fm	$-0.71 + i0.72$ fm
[10]	$-1.61 + i0.86$ fm	$0.45 + i0.62$ fm	$-0.58 + i0.74$ fm

Ref.	$a^{(0)}$	a_{K^-d}
[8]	$-0.14 + i0.59$ fm	$-1.47 + i1.08$ fm
[9]	$-0.22 + i0.70$ fm	$-1.34 + i1.04$ fm
[10]	$-0.07 + i0.68$ fm	$-1.11 + i1.30$ fm

In Fig. 1 we illustrate the K_α shift and width data obtained from all the K^-p atom measurements so far reported, as well as shifts and widths calculated from various theoretical analyses of K^-p scattering and atomic data. The recent, most reliable data from the KEK experiment [5] have an uncertainty of about 25% in the shift and 75% in the width. The expected DEAR result is also shown. Its uncertainty of about 1% in the shift and about 5% in the width will clearly discriminate various theoretical calculations and provide a strong constraint on the K^-p dynamics.

2.5 The meson-nucleon sigma terms

The K^-N scattering lengths determined by the DEAR experiment will place a strong constraint on the low-energy K^-N dynamics, and thereby will affect significantly the SU(3) description of chiral symmetry breaking. We discuss here possible consequences of the DEAR experiment on the key quantities of chiral symmetry breaking, the KN sigma terms and the strangeness content of the proton.

Quantum-Chromo-Dynamics (QCD) is regarded as the basic theory of the strong interaction. The theory possesses the important feature of asymptotic freedom: as the distance scale becomes smaller, or as the momentum transfer becomes larger, the QCD coupling constant becomes weaker and the interactions diminish. In this high-energy domain, perturbative QCD has been successfully applied. In the low-energy domain, however, the (running) QCD coupling constant becomes stronger, and the theory exhibits the confinement of color. The quarks and gluons are thus confined (this is referred to as infrared slavery), and perturbative QCD ceases to be useful for low-energy phenomena.

Because of confinement, the relevant degrees of freedom are hadrons in the low-energy domain, instead of quarks and gluons. However, the basic characteristics of the hadrons, such as spin, charge and strangeness, reflect the quantum numbers of the quarks, forming the flavor SU(3) symmetry (and its breaking). Furthermore, the use of effective (constituent) masses of the quarks provides a successful, quantitative description of the hadron mass and other properties.

Apart from SU(3) symmetry, the pattern of the hadron spectrum in nature shows a peculiar lack of symmetry. For example, while there are several pseudoscalar mesons of light mass, no light scalar mesons are observed. The pseudoscalar mesons – pions, kaons, and the eta – are considered to be Goldstone bosons, which appear through spontaneous breaking of chiral symmetry; that is, from the left-and-right $\mathrm{SU}_L(3)\times\mathrm{SU}_R(3)$ symmetry to $\mathrm{SU}_V(3)$ symmetry. Strictly speaking, the chiral symmetry and its spontaneous breaking are applicable to massless quarks. In the world we live in, the quarks are massive, and the chiral symmetry is also explicitly broken by the quark masses.

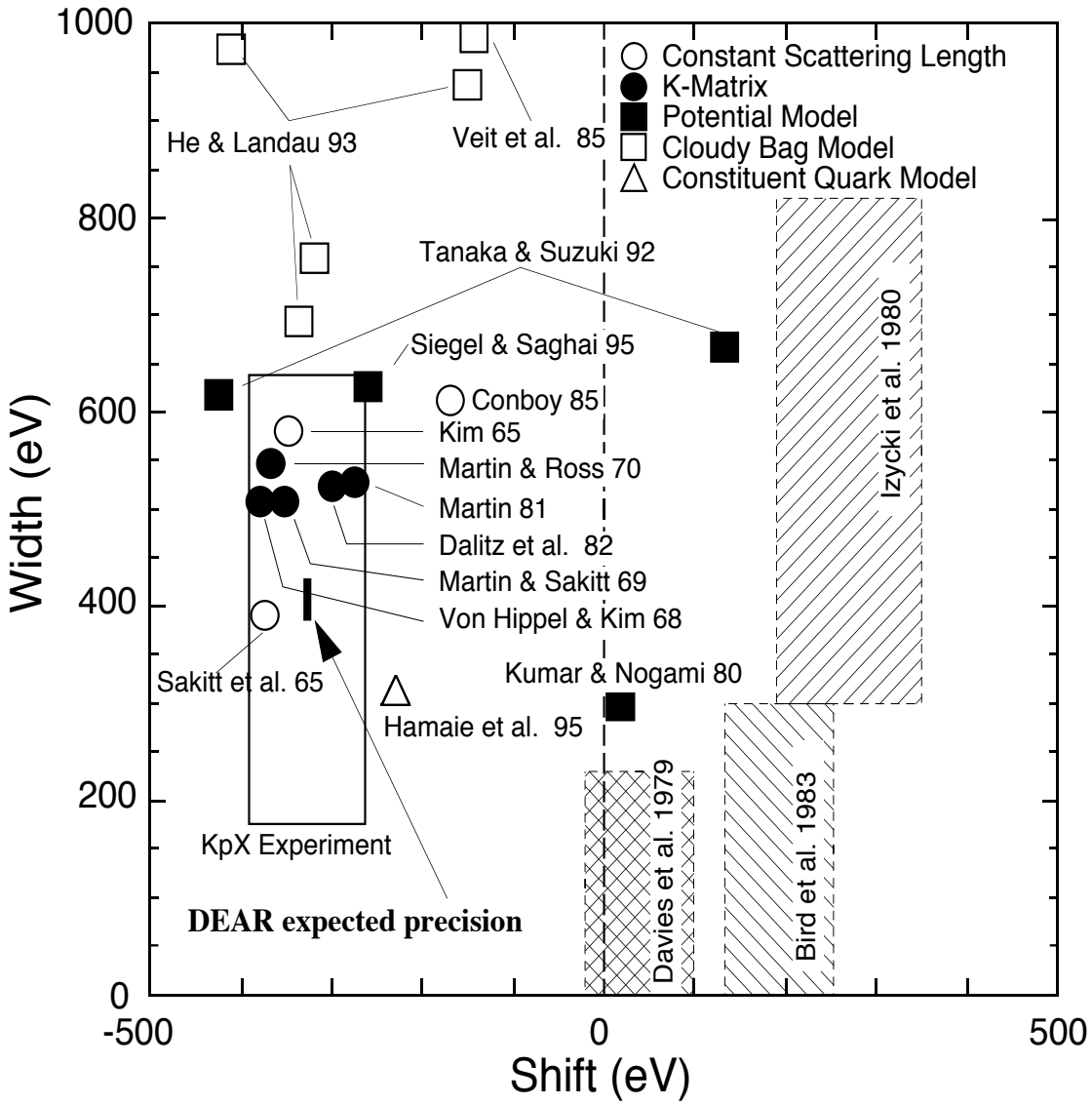

Figure 1: (reproduced from ref. [5] with the permission of the authors). Presently available data on shift and width of the K_α line of kaonic hydrogen, as obtained from kaonic hydrogen measurements or deduced from scattering data analyzed through various approaches. The DEAR expected precision is also shown.

Furthermore, the quark masses are different, $m_s >> m_u \approx m_d$, strongly disturbing the SU(3) symmetry (here, m_u, m_d, m_s are the masses of the up, down, and strange quarks, respectively). Hadron properties thus exhibit the complicated consequences of the two fundamental symmetries of QCD, SU(3) symmetry and chiral symmetry, and their breaking.

The quark masses are relatively small and could serve as parameters for perturbative expansions. Such expansions, after incorporating the symmetry properties of QCD, form a chiral perturbation theory, which has been demonstrated to be quite successful. The theory is not renormalizable, and several (in fact, a growing number of) coefficients in the theory have to be determined phenomenologically. But the expansion is systematic and, if it converges, the theory provides the best description of low-energy hadron dynamics.

Another method to treat QCD is a lattice calculation. As is well known, it deals directly with the QCD degrees of freedom, but it is limited by computer capabilities largely to a single hadron at present, as well as being plagued with difficulties in the treatment of fermions (quarks).

2.5.1 Chiral symmetry breaking and meson-nucleon sigma terms

The meson-nucleon sigma term provides a measure of the chiral symmetry breaking and is an important quantity in non-perturbative QCD. As such, it is directly related to various other quantities associated with QCD, such as condensate in high-density nuclear matter and the nucleon mass. It is especially important in connection with the strangeness content that provides the SU(3) description of the nucleons beyond the naive SU(2) description.

The meson-nucleon sigma term is defined as the expectation value of a double commutator of the chiral symmetry breaking part of the strong-interaction Hamiltonian, H_{SB},

$$\sigma_N^{ba} = i < p|[Q_b^5, [Q_a^5, H_{SB}]]|p > \quad , \tag{18}$$

with the proton state $|p >$ of momentum p [11]. Here, Q_a^5 is the axial-vector charge with the SU(3) index a. Q_a^5 and the SU(3) vector charges form the chiral left-and-right SU$_L$(3)×SU$_R$(3) algebra. Furthermore, the divergence of the axial-vector current, $\partial_\mu A_a^\mu$, associated with Q_a^5, is identified with the pseudoscalar meson fields through the partially conserved axial vector current (PCAC) hypothesis.

When these are applied, the double commutator is replaced by a product of two meson fields – two $\partial_\mu A_a^\mu$'s. The term σ_N^{ba} is thus directly related to the meson-nucleon scattering amplitude $T_{ba}(\nu, t, q^2, q'^2)$, in the limit $\nu = (s-u)/2M = 0$, $t = 0$, and the meson momenta $q^2, q'^2 \to 0$:

$$\sigma_N^{ba} = -f_a f_b T_{ba}(0,0,0,0). \tag{19}$$

Here, $s, t,$ and u are the Mandelstam variables, and the f's are meson decay constants.

σ_N^{ba} is symmetric in the SU(3) indices and, as seen above, is basically the expectation value of the two (b, a) meson fields with the proton state of isospin 1/2. The meson-nucleon sigma terms are then labeled by the combined isospin of the meson and the anti-meson, that is, the isospin of the meson-nucleon scattering amplitude in the symmetric t-channel. Consider, for example, πN scattering. The isospin in the t-channel – the total isospin of two pions – is either 0 or 2, but only the isospin zero state contributes because the nucleon isospin is 1/2. On the other hand, the kaon has isospin 1/2, and the symmetric t-channel isospin of the KN system is 0 and 1, both of which can contribute. Thus we have two KN sigma terms.

H_{SB} is usually taken to be a sum of the SU(3) singlet term, H_0, and the octet term, H_8:

$$H_{SB} = H_0 + H_8. \tag{20}$$

While H_0 preserves the SU(3) symmetry, H_8 breaks it.

In quark language [12], H_{SB} is the quark mass term,

$$\begin{aligned} H_{SB} &= m_u \bar{u}u + m_d \bar{d}d + m_s \bar{s}s & (21) \\ &\approx \frac{1}{3}(m_s + 2\bar{m})(\bar{u}u + \bar{d}d + \bar{s}s) - \\ &\quad \frac{1}{3}(m_s - \bar{m})(\bar{u}u + \bar{d}d - 2\bar{s}s) = H_0 + H_8, & (22) \end{aligned}$$

where, at the second step, the isospin invariance $m_u = m_d = \bar{m}$ is assumed. Here, m_u, m_d, and m_s are the quark-mass parameters appearing in the QCD Lagrangian. With this, the πN sigma term is expressed as [12]:

$$\sigma_{\pi N} = \bar{m} < p| \ \bar{u}u + \bar{d}d \ |p> . \tag{23}$$

For the KN system, exact expressions for the two sigma terms, characterized by the symmetric t-channel isospin 0 and 1, are [12]:

$$\begin{aligned} \sigma_{KN}^{(1)} &= \frac{1}{2}(\bar{m} + m_s) < p| \ \bar{u}u + \bar{s}s \ |p> & (24) \\ \sigma_{KN}^{(0)} &= \frac{1}{2}(\bar{m} + m_s) < p| \ -\bar{u}u + 2\bar{d}d + \bar{s}s \ |p> . & (25) \end{aligned}$$

2.5.2 Determination of the kaon-nucleon sigma terms

After long debates involving chiral perturbation calculations and phenomenological analyses, a consensus [13] seems to have been reached on the value of the πN sigma term:

$$\sigma_{\pi N} \approx 45\,\mathrm{MeV}, \tag{26}$$

with an uncertainty of a few MeV.

The situation with the KN sigma terms is more unclear. Various calculations based on chiral perturbation theory as well as phenomenology have yielded different values, scattered over several hundred MeV. Each has its own problems, resulting in substantial uncertainties.

Chiral perturbation theory (CHPT) gives [14]

$$\sigma_{KN}^{(1)} = 200 \pm 50\,\mathrm{MeV} \tag{27}$$

$$\sigma_{KN}^{(0)} = 140 \pm 40\,\mathrm{MeV}, \tag{28}$$

calculated to the order q^3 (q is the small momentum parameter appearing in the theory). The calculation treats the baryons as heavy fermions, and the σ_{KN} values are based on the $\sigma_{\pi N}$ value quoted above (26), in addition to various low-energy constants and baryon masses.

A more recent CHPT calculation reports [15],

$$\sigma_{KN}^{(1)} = 380 \pm 40\,\mathrm{MeV}\ , \tag{29}$$

$$\sigma_{KN}^{(0)} = 250 \pm 30\,\mathrm{MeV}\ . \tag{30}$$

In this calculation, the convergence of the perturbative expansion is examined by comparing two regularization methods, cutoff and (commonly used) dimensional regularization. The convergence of SU(3) chiral perturbation theory is found to be problematic when baryons are involved [16].

The sigma terms are physical quantities hence their values must be independent of how they are computed, that is, of the regularization scheme. The issue of convergence must be resolved for this approach to be reliable. Furthermore, there is the question of decuplet contributions, which were not included in the calculation of Eqs. (27) and (28).

Phenomenological determination of the KN sigma terms was actively pursued in the 1970's, with the most recent analysis reported in 1981. The commonly used procedure is as follows [17]:

1) Apply a dispersion relation, and obtain the Kp scattering amplitude at the Cheng-Dashen point,

$$T(0, 2m_K^2, m_K^2, m_K^2), \tag{31}$$

which is on the mass shell but unphysical ($t > 0$). The dispersion relation used is a once-subtracted and fixed-t dispersion relation.

2) Invoke a smoothness assumption, extrapolate the amplitude from the Cheng-Dashen point to the zero-momentum point where these kinematic variables all vanish. The KN sigma terms are then obtained from Eq. (19).

The Cheng-Dashen point is favored because all Born pole terms vanish (due to the choice of pseudoscalar couplings to satisfy PCAC) and also the Adler consistency condition provides a constraint. The procedure requires both K^+p and K^-p cross sections and sub-threshold contributions, because the Kp dispersion relation is formulated to satisfy the crossing relation.

The second step may involve non-analytic extrapolation as chiral perturbation theory indicates [14, 15], but the numerical consequence of the non-analyticity is as yet unclear. A different approach – the use of the unitarity condition – has also been proposed [18, 19] to achieve a more reliable result. Chiral perturbation theory could provide a convenient means for the extrapolation once the issue of convergence is resolved.

The phenomenological procedure involves a large uncertainty caused by poorly determined observables. Apart from those due to the extrapolation, the major uncertainties come from [20]:
a) the $K^{\pm}p$ scattering lengths and
b) the coupling strengths of the pole and resonance contributions.
Now that KN sigma terms with smaller uncertainties have been reported, critical examination of the phenomenological procedures was made in 1979 and 1981 [20], the results of which may be summarized as:

$$\sigma_{KN}^{(1)} \simeq 600 \pm 400\,\mathrm{MeV}. \tag{32}$$

Since that time, many key observables used in the previous calculations have become better known:
a) The crucial s-wave, $I(\mathrm{isospin}) = 0$, $\Lambda(1405)$ mass and width are determined [21] to within a few tenths of a percent and a few percent, respectively. The important p-wave, $I = 1$, $\Sigma(1385)$ parameters are even better known [22] than the $\Lambda(1405)$ parameters.
b) The 1983 compilation of coupling constants and low-energy parameters [23] reports substantially better determined values than those in previous compilations.
c) More reliable K^+N phase shifts up to 700 MeV in the center-of-mass energy have become available, and the KN scattering lengths have been determined to within 3 % and 10 % for $I = 1$ and 0 states, respectively [24].
d) The K^-p s-wave scattering length has been determined with an accuracy of about 30% by the recent KEK experiment [5].

When the DEAR K^-N scattering lengths of a few percent precision become available, the s-wave K^-N amplitudes will be determined more accurately below and above threshold, as well as their couplings to the other channels.

Furthermore, the precise s-wave information will provide a tighter constraint on the determination of the p-wave parameters from experimental data. The p-wave information

is important when the fixed $t(=2m_K^2)$ dispersion relation is used to reach the Cheng-Dashen point directly. It is also possible, however, to use the forward ($t=0$) dispersion relation to reach the Cheng-Dashen point through the on-mass $(\nu,t)=(0,0)$ point [25].

In either case, the DEAR experiment will have a strong impact on reducing the error in the phenomenological determination of the KN sigma terms. It is difficult to make a quantitative assessment of the impact. However, based on the above discussions, we expect that the KN sigma terms could be determined to the order of 20 % by combining DEAR results with the significantly improved post-1981 information on low-energy $K^{\pm}N$ interactions.

Finally, we note a recent KN sigma term calculation using K^--nucleus interactions from kaonic atom data. It is based on a dispersion relation approach originally due to Fubini and Furlan. The calculation gives [19, 26]

$$\sigma_{KN}^{'} = \frac{1}{4}(3\sigma_{KN}^{(1)}+\sigma_{KN}^{(0)}) = 512 \pm 101 \ \mathrm{MeV} \tag{33}$$

$$\sigma_{KN}^{''} = \frac{1}{2}(\sigma_{KN}^{(1)}-\sigma_{KN}^{(0)}) \leq 78 \ \mathrm{MeV}. \tag{34}$$

The uncertainties do not include those due to the various assumptions in the approach, associated with the use of complex nuclei.

2.5.3 The strangeness content of the proton and the sigma terms

The naive quark model describes the nucleons as consisting primarily of up and down quarks. Recent work on the nucleon structure functions from spin-dependent deep inelastic scattering [27, 28, 29, 30] has demonstrated that the spin [31, 32], and magnetic moment [33] of nucleons cannot be fully understood by "valence" quark models based on the SU(2) scheme. We note that several parity-violating electron scattering experiments are either underway or planned at MIT-Bates [34], TJNAF [35], and Mainz [36], to find the strangeness content of the magnetic moments of the nucleons. The SU(3) structure of the nucleons appears more explicitly in the quantities associated with chiral symmetry breaking.

The fraction of the strangeness contribution (the strange fraction) in the proton is defined as:

$$y = \frac{2<p|\bar{s}s|p>}{<p|\bar{u}u+\bar{d}d|p>}. \tag{35}$$

These quark expectation values can be expressed in terms of the πN and KN sigma terms by inverting Eqs. (23)-(25). The strange fraction is then written as

$$y = \frac{4\bar{m}}{\bar{m}+m_s}\frac{\sigma_{KN}^{\prime}}{\sigma_{\pi N}} - 1, \tag{36}$$

where σ'_{KN} is defined in Eq. (33). Note that $4\bar{m}/(\bar{m}+m_s) \approx 0.15$ by the use of $m_s/\bar{m} \approx 2m_K^2/m_\pi^2 \approx 25$ from PCAC analysis of meson masses [37].

Equation (36) shows that the πN and KN sigma terms contribute to the strangeness fraction in the opposite ways, but with the equal weight. As noted previously, however, the πN sigma term is much better determined. With the proton expectation value for H_8 of Eq. (22), the SU(3) breaking octet term, the πN sigma term is related to the strange fraction by

$$(1-y)\sigma_{\pi N} = -\frac{3\bar{m}}{m_s-\bar{m}} < p|H_8|p > . \tag{37}$$

The strange fraction compatible with $\sigma_{\pi N}$ of Eq. (26) has been found to be [13, 38]:

$$y \simeq 0.2 . \tag{38}$$

These values give the strangeness contribution to the proton mass,
$m_s \partial m_N/\partial m_s = m_s < p|\bar{s}s|p > \simeq$ 130 MeV, where the Feynman-Helman theorem has been applied in the second step.

How sensitive is y to the $\sigma_{\pi N}$ and σ_{KN} values? This is a complicated question since y also depends on other quantities. Jaffe and Korpa [39] have compared various scenarios under different assumptions. We excerpt some of their comparisons in Table 2. The table shows that the strange fraction is quite sensitive to the KN sigma term.

Table 2: Sensitivity of $\sigma_{\pi N}$ and σ_{KN} to y [39]. σ'_{KN} is defined in Eq. (33).

$\sigma_{\pi N}$ (MeV)	y (%)	σ'_{KN} (MeV)
51	48	490
51	2	360
27	0	170

2.5.4 Impact of the DEAR experiment

An accurate measurement of the strong-interaction shifts and widths in both K^-p and K^-d atoms (1 % in K^-p shift but less accurate for K^-d shift and for both widths) would provide:

1. the s-wave K^-N scattering lengths to within a few percent uncertainty;
2. a more precise determination of the multi-channel K^-N scattering amplitudes above and below the threshold, including $\Lambda(1405)$;

3. a KN sigma term determination to the order of 20 % uncertainty;

4. a better determination of the strangeness content of the proton.

References

[1] S. Deser *et al.*, Phys. Rev. **96** (1954) 774;
T.L. Truemann, Nucl. Phys. **26** (1961) 57;
A. Deloff, Phys. Rev. **C13** (1976) 730.

[2] J.D. Davies *et al.*, Phys. Lett. **B83** (1979) 55.

[3] M. Izycki *et al.*, Z. Phys. **A297** (1980) 11.

[4] P.M. Bird *et al.*, Nucl. Phys. **A404** (1983) 482.
(1997) 3067.

[5] M. Iwasaki *et al.*, Phys. Rev. Lett. **78** (1997) 3067;
S.N.Nakamura *et al.*, Nucl. Inst. and Meth. **A408** (1998) 438;
T.M.Ito *et al.*, Phys. Rev. C **58** (1998) 2366.

[6] R. Seki, Phys. Rev. **182** (1969) 1773.

[7] A.W. Thomas and R.H. Landau, Phys. Rep. **3** (1980) 121.

[8] G. Toker, A. Gal and J.M. Eisenberg, Nucl. Phys. **A362** (1981) 405.

[9] M. Torres, R.H. Dalitz and A. Deloff, Phys. Lett. **B174** (1986) 213.

[10] A. Bahoui *et al.*, Nucl. Phys. **A508** (90) 335c.

[11] H. Pagels, Phys. Rep. **16** (1975) 219; E. Reya, Rev. Mod. Phys. **46** (1974) 545.

[12] J. F. Gunion, P. C. McNamee, and M. D. Scadron, Nucl. Phys. **B 123** (1977) 445.

[13] J. Gasser, H. Leutwyler and M.E. Sainio, Phys. Lett. **B253** (1991) 252, 260.

[14] V. Bernard, N. Kaiser and U.-G. Meissner, Z. Phys. **C60** (1993) 111.

[15] B. Borasoy, hep-ph/9807453 (1998).

[16] J. Donoghue, B. Holstein, and B. Borasoy, hep-ph/9804281 (1998); J. Donoghue and B. Holstein, hep-ph/9803312 (1998).

[17] E. Reya, Phys. Rev. **D7** (1973) 3472.

[18] P. M. Gensini, J. Phys. **G 7** (1981) 1177;

[19] P. M. Gensini, hep-ph/9804344 (1998).

[20] B. Di Claudio, G. Violini and A.M. Rodriguez-Vargas, Lett. Nuovo Cimento **26** (1979) 555; A. D. Martin and G. Violini, Nuovo Cimento **30** (1981) 105.

[21] R. H. Dalitz and A. Deloff, J. Phys. **G 17** (1991) 289; (E) **G 19** (1993) 1423.

[22] Particle Data Group, Eur. Phys. J. **C 3** (1998) 695.

[23] O. Dumbrajs *et al.*, Nucl. Phys. **B 216** (1983) 277.

[24] T. Barnes and E.S. Swanson, Phys. Rev. **C49** (1994) 1166.

[25] N. F. Nasrallah and K. Schilcher, Phys. Rev. **D7** (1973) 810.

[26] P.M. Gensini, Il Nuovo Cimento **60A** (1980) 234.

[27] EMC Collaboration, J. Ashman *et al.*, Nucl. Phys. **B328** (1989) 1.

[28] E142 Collaboration, P.L. Anthony *et al.*, Phys. Rev. Lett. **71** (1993) 959.

[29] SMC Collaboration, B. Adeva *et al.*, Phys. Lett. **B302** (1993) 533.

[30] SMC Collaboration, D. Adams *et al.*, Phys. Lett. **B329** (1994) 399.

[31] E143 Collaboration, K. Abe *et al.*, Phys. Rev. Lett. **74** (1995) 346.

[32] T. Hatsuda and T. Kunihiro, Nucl. Phys. **B387** (1992) 715; R. Decker, Th. Leize and M. Novakowski, Phys. Lett. **B244** (1990) 497; R. Jaffe and A. Manohar, Nucl. Phys. **B337** (1990) 509.

[33] B.L. Ioffe and M. Karliner, Phys. Lett. **B247** (1990) 387; H. Fritzsch, Phys. Lett. **B256** (1991) 75; W. Koepf, E.M. Henley and S.J. Pollock, Phys. Lett. **B228** (1992) 11; M.J. Musolf and M. Burkardt, Z. Phys. **C61** (1994) 433.

[34] B. Mueller *et al.*, Phys. Rev. Lett. **78** (1997) 3824; private communication with R. McKeown.

[35] TJNAF experiments E91-017 (D. Beck, spokesperson): E91-010 (P. Souder and J. Finn, spokesperson): E91-004 (E. J. Beise, spokesperson).

[36] Mainz Proposal A4/1-93, 94-11 (D. von Harrach, spokesperson).

[37] T.-P. Cheng and L.-F. Li, *Gauge Theory of Elementary Particle Physics* (Clarendon Press, Oxford 1984) Section 5.5.

[38] J. Gasser and H. Leutwyler, Phys. Rep. **87** (1982) 77; J. Gasser, Ann. Phys. (NY) **136** (1981) 62.

[39] R.L. Jaffe and C.L. Korpa, Comments Nucl. Part. Phys. **17** (1987) 163.

3 Experimental overview

3.1 The principle of the experiment

The principle of the DEAR experiment is very simple: low-momentum negative kaons, produced by the decay of ϕ mesons created by e^+e^- collisions in the interaction point of one of the two straight sections of DAΦNE, leave the beam pipe through a thin window, are degraded in energy down to a few MeV, enter a gaseous hydrogen (deuterium) target placed several centimeters above the pipe and are stopped there. Some of the kaons are captured in an outer orbit of the atoms, thus forming exotic kaonic hydrogen (deuterium) atoms. The kaon then cascades down through a series of bound atomic states until it reaches a level where the short-range strong interaction causes its absorption.

A suitable soft X-ray detector, such as the Charge Coupled Device (CCD) detector, allows us to measure the energy of the X rays emitted in transitions to the $1s$ state (the K-series lines). Subtracting the QED-determined electromagnetic energy yields the shift of the $1s$ level caused by the strong $\bar{K}N$ interaction.

3.2 The experimental setup

A pictorial view of the DEAR experimental setup is shown in Figure 2.

3.2.1 The kaon source

The DEAR experiment was designed taking the characteristics of the DAΦNE "kaon beam" into account. Kaon pairs are produced by the decay of the ϕ-meson with a branching ratio of 49.5%. The width of the ϕ resonance is approximately 4.4 MeV; however, it is not this width that determines the momentum spread of the kaons produced, but rather, the energy spread of the accelerator itself, which is projected to be on the order of 0.4 MeV. Thus, the two-body decay of ϕ-mesons at DAΦNE produces low momentum (127 ± 1.2 MeV/c) kaons, emitted with a $\sin^2\theta$ distribution with respect to the beam pipe axis, and isotropically with respect to the orthogonal angle around the beam pipe axis.

3.2.2 The beam pipe

A special beam pipe, to be centered at one of the DAΦNE interaction points, was manufactured for the experiment. It consists of a thin (250 μm) aluminum pipe, 690 mm long, with a 650 μm layer of carbon fiber reinforcement. The inner diameter of the pipe is 90.00 ± 0.01 mm. A plastic scintillator degrader, 300 mm long, 2.35 mm thick, is placed around the pipe in order to slow the kaons.

A pipe constructed of beryllium would further reduce the effects of multiple scattering. However, the flexibility (hence safety) and cost more than justify the chosen design.

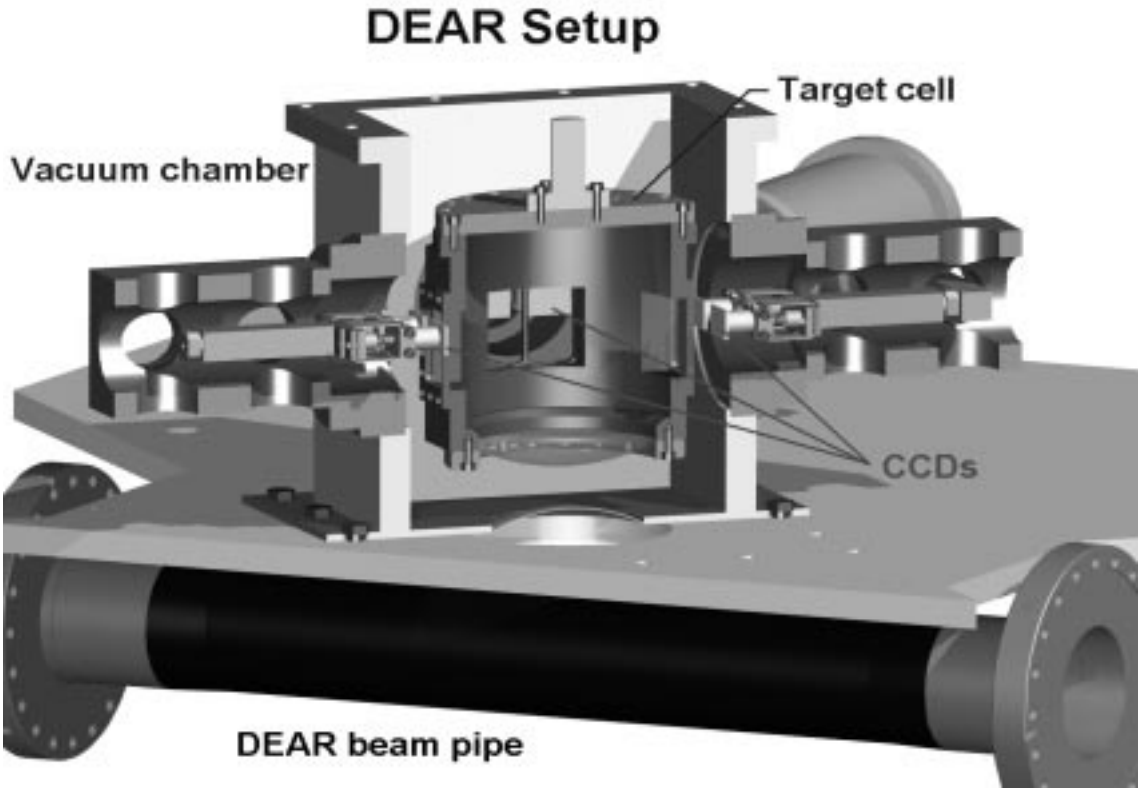

Figure 2: The DEAR experimental setup

3.2.3 The cryogenic target

To achieve a balance between high kaon stopping density in the target cell and the decreasing X-ray yield due to Stark mixing, a pressurized cryogenic gaseous target must be used. The requirements of the target system are:

- temperature range 20 to 30 K;
- pressure range 1 to 3 atm;
- gas purification to maintain impurity level below 1 ppm;
- only low Z materials used around the CCD detectors;
- hydrogen safety requirements must be met;
- accurate positioning of the target cell.

To satisfy these requirements, an apparatus using a cryogenic refrigerator for cooling the target cell, a wide-range turbomolecular pump for maintaining the necessary insulation vacuum and a storage and purification unit for the hydrogen gas used in the experiment was designed. The setup of the cryogenic target is shown in Figure 3.

The initial target conditions will be a hydrogen pressure of 3 atm and temperature of 25 K. This will result in a target density of 3.6×10^{-3} g/cm^3 ($\simeq\ 32\ \rho_{STP}$). According to cascade calculations [1], the expected yield of K_α X rays per stopped kaon in these conditions is $(1-3)\%$, depending on the selected values of the cascade parameters.

3.2.4 The cryogenic refrigerator

A two-stage closed-cycle cryogenic refrigerator with helium gas as the exchange medium (APD-Cryogenics DE-204SLB) is used to cool the target cell. The cooling power at 20 K is 6.75 Watts. The typical cooling time is approximately 15 hours. A radiation shield surrounds the target cell and the refrigerator head. The shield is made of ten layers of "super-insulation" (aluminized mylar). The temperature of the target cell is measured at the cold end of the refrigerator and on the bottom of the cell with silicon diode temperature sensors. A LakeShore temperature controller is used to stabilize the target temperature to within ± 0.2 K in the range 20-30 K.

The pressure in the insulation vacuum chamber must be less than 10^{-5} mbar to obtain the necessary vacuum for cryogenic work. Therefore a wide-range turbomolecular pump (Varian 300 HT) with a pumping speed of 300 l$\cdot$s^{-1}, is used, thus achieving an insulation vacuum of 10^{-7} mbar.

3.2.5 The vacuum chamber and the target cell

The material for making the vacuum chamber and the target cell was selected very carefully, because the most common materials used for cryogenic systems, such as stainless

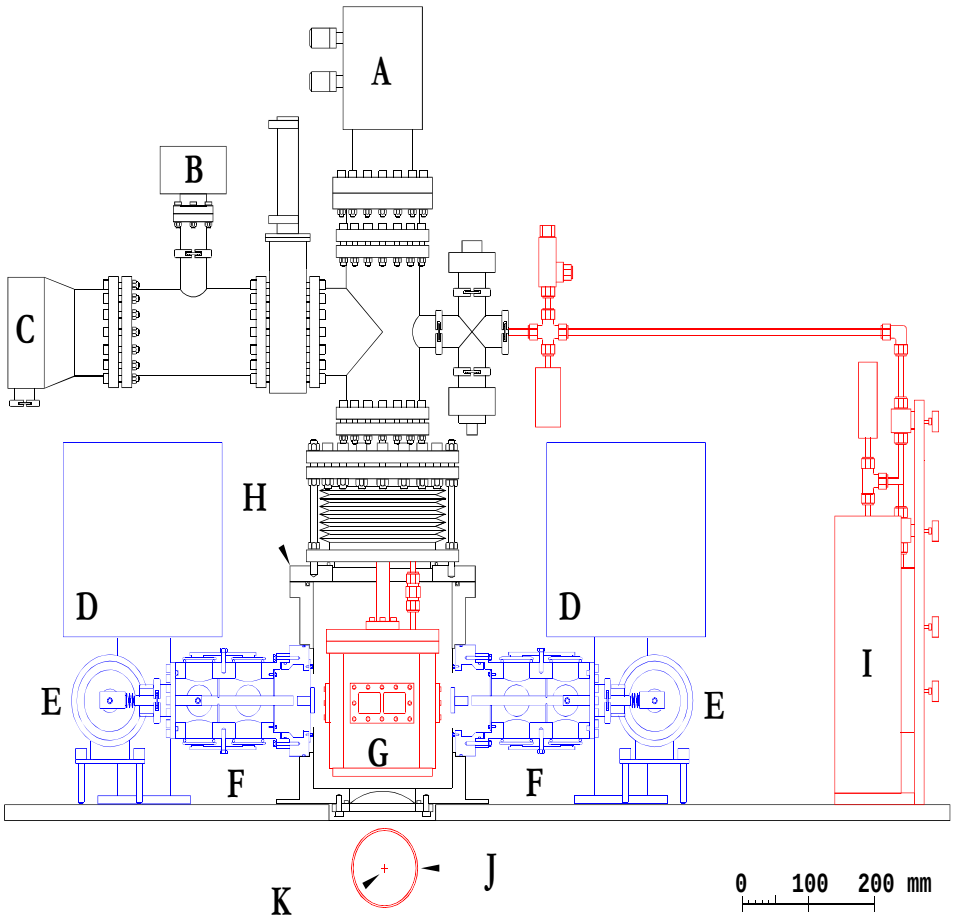

Figure 3: The DEAR cryogenic target setup: A APD cryosystem for the target cell; B Quadrupole mass spectrometer; C Turbomolecular pump; D CCD readout electronics; E CCD cryosystem; F CCD vacuum chambers; G Target cell; H Target cell insulation vacuum chamber; I Hydrogen storage; K Interaction point; J Beam pipe.

steel and copper, cannot be used in a kaonic hydrogen experiment due to their characteristic electronic X rays in the energy region of interest. Therefore, an aluminium alloy (AlMgSi 0.5) with a low manganese content (less than 0.1%) was selected for the construction of the target cell and the vacuum chamber.

The insulation vacuum chamber is a hollow cube ($230 \times 230 \times 240$ mm^3, wall thickness of 15 mm) with the kaon entrance window at the bottom and 100 mm diameter ports on each side wall to mount the CCD vacuum chambers. The kaon entrance window is made of 100 μm thick aluminium and is O-ring-sealed to the vacuum chamber. The refrigerator head is flanged with standard ISO-K components via an edge-welded bellows on the top of the cubic vacuum chamber. This configuration allows one to make a fine adjustment of the target cell within the vacuum chamber and to properly align the cell relative to the CCDs.

The target cell is placed at $\theta = 90^o$ with respect to the beam axis. It consists of a cylinder with an inner diameter of 135 mm and a height of 160 mm. A Hostaphan foil (116 mm diameter, 150 μm thick) at the bottom of the target cell serves as an entrance window for kaons.

The lateral surface of the target cell has eight windows open to the CCD chips. Each detector system consists of two CCD chips, each with an effective area of 26×17 mm^2. The target windows are larger (30×55 mm^2) to allow for misalignments and to gain in solid angle. The windows are 50 μm Kapton sealed with indium between a window frame and the target cell.

The target cell is thermally shielded with ten layers of "super-insulator". However, the kaon entrance window is shielded with two layers, and the CCD windows are kept free.

The maximum working pressure of the target cell, including a safety factor of 2.5, is limited to 4 atm, due to the CCD window thickness. The working pressure is 3 atm.

The distance between the entrance window of the vacuum jacket and the beam-beam interaction point is 75 mm, and the distance from this window to the target entrance window is 35 mm. The distance from the bottom of the target cell to the center of each CCD pair is 80 mm, and corresponds to the mean position of the stopped K^-s, thus maximizing the acceptance for the emitted X rays. Finally, the distance between the CCD surface and the target cell is 15 mm. Details of the CCD detection system are given in the following chapter.

3.2.6 The gas handling system

Only metal fittings and metal bellows valves are used for the gas handling system. The tubing is made of stainless steel (SS316L) or copper. The whole system is heated to 200^0 C during the cleaning procedure. A high vacuum pumping system (Alcatel, Drytel 31), with an ultimate pressure of 10^{-6} mbar, must be used.

The apparatus consists of two main parts: the hydrogen purification unit and the hydrogen storage device. Hydrogen with low isotopic deuterium concentration (less than 5 ppm) is used. The hydrogen-1 isotope (protium) is produced via the electrolysis of

deuterium depleted water. The gas produced is stored as a metal hydride in a stainless steel container. The metal alloy for storing the hydrogen gas is LaNiAl. The storage capacity of this unit is 2000 liters of gas (STP) with an equilibrium pressure of 1.5 atm at room temperature (and 5 atm at 70^0 C).

To avoid additional background from X rays produced by kaons stopped in atoms other than hydrogen, the hydrogen gas is purified by means of a palladium diffusion unit. The palladium tube must be heated to 400^0 C. At this temperature, only hydrogen gas permeates through the tube at a reasonably high rate (approximately 150 cm^3s^{-1} at a pressure difference of 3 atm), while all other gases have a diffusion rate six orders of magnitude less. With this unit, the required impurity level of less than 1 ppm will be achieved.

References

[1] T. Koike, T. Harada and Y. Akaishi, Phys. Rev. **C53** (1996) 79.

4 CCDs (Charge-Coupled Devices)

4.1 Introduction

The CCD concept [1] was proposed in 1970 by Boyle and Smith [2]. The essential feature of their scheme was to store information in the form of electrical charge packets in potential wells within a semiconductor. These potential wells could be created by the influence of overlying electrodes separated from the semiconductor by a thin insulating layer. The potential wells, and therefore the charge packets, could be shifted through the semiconductor by applying phased voltages to the electrodes, providing a means of extracting the stored information. It was soon realized that charges created by incident photons could be collected and read out, giving birth to the CCD as an image sensor.

Present day CCDs, as are used in the DEAR experiment, are typically silicon based MOS (metal-oxide semiconductor) devices with a pixel structure [1,3]. In standard devices, three electrodes are required for each row of pixels, which are divided into columns by channel stops in the semiconductor. When a CCD is in accumulation mode, a negative voltage is applied to two electrodes and a positive voltage to the third, creating independent potential wells in each pixel. During the readout, alternating potentials are applied to these three electrodes, shifting the accumulated electrons to a special readout line at the end of the columns.

Although CCDs were initially developed for detecting visible light and were intended to be used mainly in video cameras [4], they are also very good low-energy X-ray detectors, leading to applications in X-ray spectrometry, as in the DEAR experiment, and in X-ray astronomy [5]. The low energy detection threshold of the CCDs is limited to about 1 keV by the thickness of the electrodes and the efficiency of the CCDs starts to decrease above a few keV because of the depletion depth of the devices and the low atomic number of the silicon used in their construction. Variations in the detector efficiency are further intensified by a 1.84 keV absorption edge in silicon. Once the detector efficiency has been understood, the CCDs are ideal for a wide range of applications in the energy range from 1-20 keV.

Work started on X-ray detection with CCDs in Neuchâtel in 1986 and the first prototype system was working in 1988. Since then, the reliability, energy resolution and background suppression algorithms of the CCD systems have been improved. Previous collaborations using the CCD detectors have measured pionic and muonic X rays at PSI (Paul Scherrer Institute) and antiprotonic X rays at CERN (LEAR). References to the development work done in Neuchâtel are given in [6].

The CCDs used in the DEAR experiment [7] consist of $770 \times 1152 = 887040$ pixels, split into two independent halves, which are read out separately. Each pixel is $22.5\ \mu$m $\times$ $22.5\ \mu$m in size, giving an area of $\approx 17 \times 26$ mm^2 ≈ 4.5 cm^2, a factor of 20 larger than the CCDs originally used in Neuchâtel's pioneering work.

4.2 Energy resolution

The energy resolution of a CCD (ΔE) is well-modelled by the expression:

$$\Delta E(\mathrm{FWHM}) = 2.355 \times \omega \, (N^2 + \frac{FE}{\omega})^{1/2} \tag{39}$$

with

ω = conversion energy for an electron-hole pair: 3.68 eV in silicon
N = r.m.s. transfer and readout noise in equivalent number of electrons
F = Fano factor $\approx$ 0.12 for silicon
E = X-ray energy

Energy resolutions (FWHM) measured in-beam during previous experiments are given in Table 3:

Table 3: CCD measured energy resolution

X-ray energy (keV)	energy resolution (FWHM) (eV)
2	$\leq$ 120
3	140 - 150
6	$\approx$ 170
8	$\approx$ 190

Using Eq. (39) and the above data, N can be calculated and is found to be equivalent to 10 to 15 electrons r.m.s. Work in Neuchâtel has concentrated on reducing N as much as possible, but has reached the point where N is now dominated by the noise of the on-chip amplifier. Further noise reduction can be obtained by sampling a pixel several times and averaging, but this would greatly lengthen the readout time. By putting $N = 0$ in Eq. (39) the theoretical limit of the energy resolution can be calculated. This limit is $\approx$ 70 eV FWHM at 2 keV and $\approx$ 140 eV FWHM at 8 keV. CCDs with a new low-noise on-chip amplifier (equivalent to 3-5 electrons r.m.s.), which will allow near theoretical limit resolution, are presently being tested by the manufacturer.

4.3 Background rejection

Even though CCDs cannot be triggered, their background rejection capabilities are very powerful, a crucial characteristic for the extraction of a weak signal from a large background, which is one of the characteristics of kaonic hydrogen experiments. In fact, in the very low energy region in conditions typical of exotic-atom research, CCDs can have a better signal-to-background ratio than triggered Si(Li) detectors. With CCDs, all background except for soft X rays can be almost completely eliminated.

The powerful background rejection capability of CCDs relies on their good two-dimensional spatial resolution already given. This rejection capability is based on the fact

that an X ray in the 1-10 keV energy region normally deposits all of its energy in a single pixel, whereas the energy from charged particles, gammas and neutrons, which constitute the background, is normally distributed over several pixels. Indeed, an X ray with energy less than 100 keV interacts in silicon almost exclusively by the photoelectric effect. For energies up to 10-20 keV, the deposited energy is normally localized in space within the depletion layer (30 μm for the deep-depleted CCDs used in DEAR), whereas charged particles lose energy by ionization everywhere in the bulk material (some mm thick). The electrons from the electron-hole pairs created in the depletion layer cannot escape from the induced potential wells, but the electrons created in the bulk material can move freely, causing charge to be collected in multiple adjacent potential wells.

Since every pixel has eight adjacent pixels, the usual way to distinguish X rays from background events is to examine the eight neighboring pixels and confirm that the charge they contain is consistent with the noise level. If this is true, the event is considered an X ray. Therefore, a good X-ray event is defined as a single pixel with energy above the noise level surrounded by 8 pixels with signals statistically consistent with noise [8]. Using this single pixel criterion and other cuts based on statistical tests of the neighboring pixels (e.g. their mean, standard deviation, etc.) it is possible to eliminate almost all background events except for soft X rays [8].

4.4 Exposure time

The accumulation period (exposure time) for the CCDs should not be so long as to permit the same 9-pixel cluster to be hit multiple times ("blindness"). If this occurs, valid X-ray events will be lost during the single pixel cut. Blindness can be caused by excessive X-ray or background events. To prevent this from occurring, the number of signal-containing pixels should not exceed $\approx$ 5%, which corresponds to approximately 4000-5000 background events per 1/2 CCD.

4.5 Detector efficiency

The total X-ray detection efficiency of the CCD system is the product of the intrinsic CCD efficiency and the probability of X-ray transmission through the hydrogen gas in the target and through the target cell windows. Intrinsic efficiency measurements for the CCDs are shown in Figure 4. Total efficiency, including windows, can in principle be modelled and measured [9,10].

4.6 Readout Electronics

The readout electronics for the CCD system consist of four major components: readout boxes, command boxes, VME crates, and data acquisition computers. A schematic representation of the CCD detector system is shown in Figure 5.

The readout boxes contain phase generators for transferring signal charges out of the CCD during a readout as well as amplifiers to (shape and) amplify the analog signal. To minimize the noise introduced by the analog sampling of the CCDs, a correlated

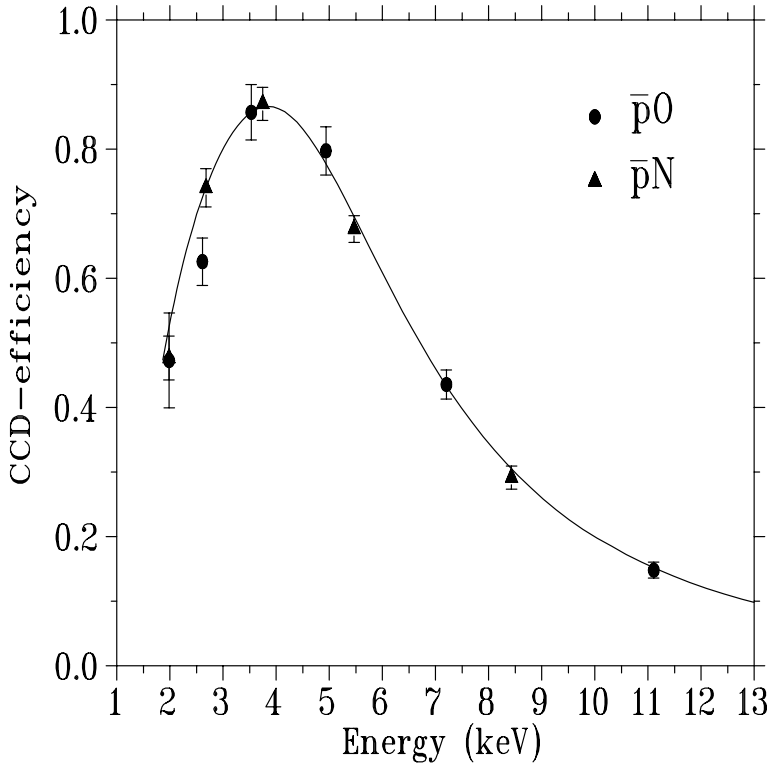

Figure 4: Intrinsic CCD efficiency. The data points are derived from measurements of relative line intensities in antiprotonic nitrogen and oxygen [9,10]. The solid curve corresponds to a calculation assuming a CCD depletion layer thickness of 30 μm.

double-sampling technique is used in which the output of the CCD is sampled with and without the signal, and the results subtracted to eliminate the constant reset level of the amplifiers [7]. This technique lengthens the readout time, but minimizes the noise such that the remaining dominant noise is the output amplifier noise. Even with this technique, the transfer and readout time is 64 μs per pixel, and since the CCD halves are read out simultaneously, the total readout time is 64 μs $\times$ 443520 $\approx$ 28 s, which is significantly shorter than the typical exposure times, and is thus not a problem since data accumulation continues throughout the readout.

The command boxes generate the logic and command signals for the readout boxes, perform the analog to digital conversion of the CCD signals, supply power to the readout boxes, and act as a communication link between the analog CCD hardware and the digital VME system.

The VME crates each contain a CCD control module and a BIT-3 VME-to-PC fiber-optic link controller. The CCD control modules are used to communicate with the command boxes and contain a buffer to temporarily store the CCD images. The BIT-3 controllers link the VME bus to the bus of the data acquisition computers.

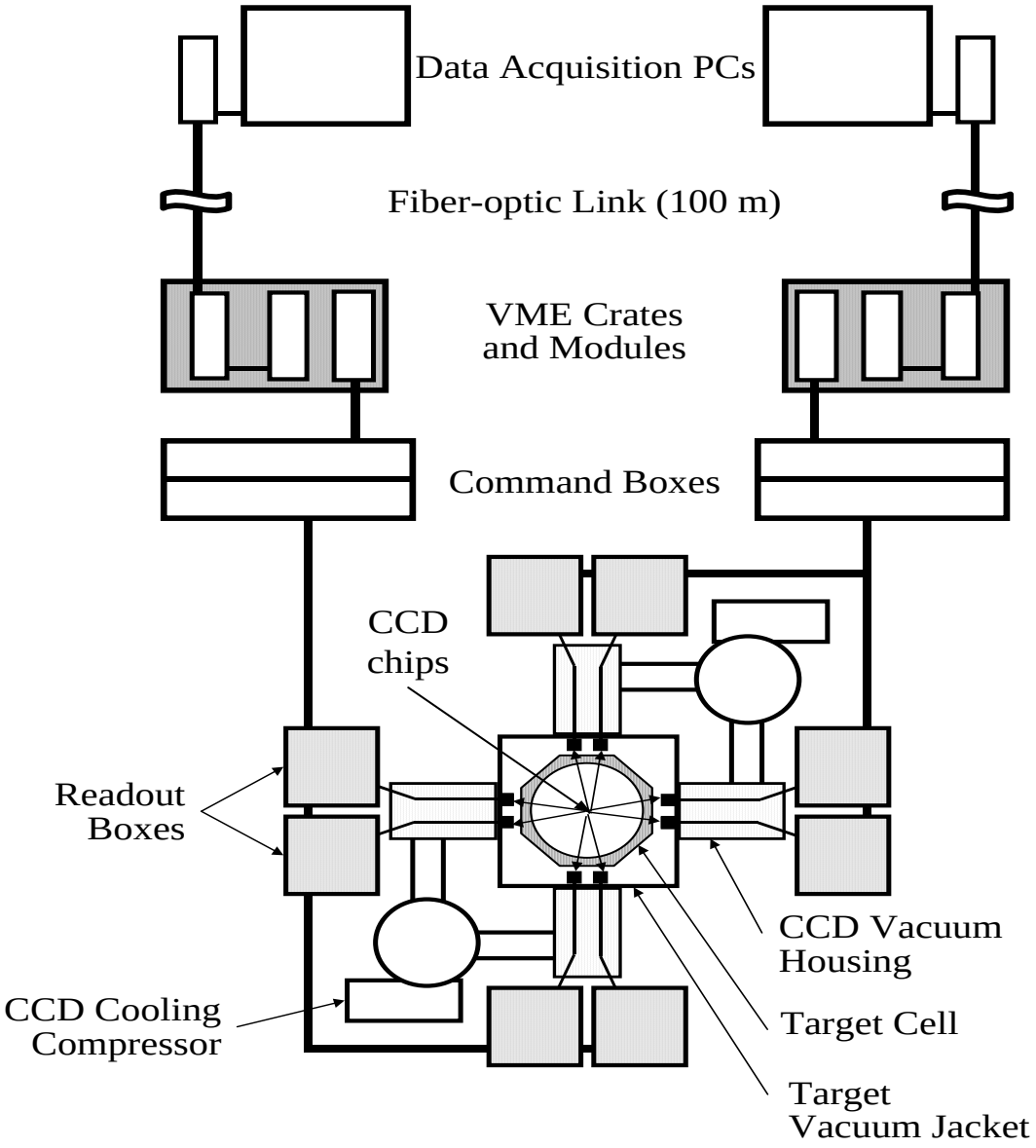

Figure 5: Block diagram of a CCD X-ray detection system with 8 CCDs.

The data acquisition computers provide a user interface to the CCD system and are used to compress, store and analyze the CCD data.

4.7 CCD cooling system

To minimize thermal noise, and thus reduce the overall noise, the CCDs should be operated at a temperature between 150 K and 180 K. The eight CCDs will be cooled by two one-stage closed-cycle refrigerators (APD "CRYOTIGER"), each with a refrigeration capacity of 20 Watts at 120 K, and the CCD temperatures will be monitored with PT-100 sensors.

In order to cool the CCDs with the available refrigeration system they must remain in an insulation vacuum of at least 10^{-3} mbar. In the final configuration, the CCDs share the insulation vacuum of the cryogenic target, with a pressure less than 10^{-6} mbar.

A monitoring and control system based on the National Instruments LabVIEW development system has been designed to monitor and record the CCD temperatures and insulation vacuum pressure as well as various other operating parameters of the system.

4.8 Data acquisition and on-line analysis

The data acquisition system used in the DEAR experiment is relatively simple. There are no triggers, fast coincidences or interrupts involved. The CCDs are simply exposed to the target for a finite length of time and the collected charges are read out, amplified, digitized, transferred to computer, compressed, and stored for future analysis.

The CCD system hardware has only two commands: CLEAR and READ. Both commands cause all the charges stored in a CCD to be transferred out of the CCD. In the case of a CLEAR command, the transfer is extremely fast and the charges, which are distorted by the poor transfer efficiency caused by the rapid transfer, are not amplified but are simply removed from the CCD. In the case of a READ command, the transfer is much slower, maintaining a high transfer efficiency, and the charges are amplified, digitized and transferred to the computer. When neither command is being performed, the CCDs are in accumulation mode, simply collecting electrons that are liberated in the process of electron-hole pair creation into the potential wells of the pixels. Typically, a data set consists of hundreds or thousands of readouts, which can be automated by the data acquisition software to occur at regular intervals.

In addition to the data acquisition software, three other programs have been written for the purpose of on-line analysis: an image viewer, a preanalysis program, and a simple analysis program. The image viewer displays the CCD images in false color and calculates some basic statistics, including noise level, number of potential signal events, and CCD occupancy: the last of these is particularly important for determining appropriate CCD exposure times. The preanalysis program calculates and subtracts the noise level (pedestal), performs a relaxed single-pixel cut, and saves the potential events into files. The analysis program reads in files produced by the preanalysis program, possibly from multiple readouts, allows cuts to be made on various parameters, and performs basic fits.

The online analysis is quite fast and can usually be performed between readouts.

References

[1] J.D.E. Beynon and D.R. Lamb, *Charge-coupled devices and their applications*, McGraw Hill (London) 1980.

[2] W.S. Boyle and G.E. Smith, *Charge-coupled semiconductor device*, Bell Syst. Tech. Journal **49** (1970) 587.

[3] G. Charpak and F. Sauli, Ann. Rev. Nucl. Part. Sci. **34** (1984) 285.

[4] R.L. Rodgers, *Charge-coupled imager for 525-line television*, Digest of IEEE Intercon, March 1974, Session 2.

[5] J.L. Culhane, Nucl. Instr. and Meth. **A310** (1991) 1.

[6] J.-P. Egger, D. Chatellard and E. Jeannet, *Progress in soft X-ray detection: The case of exotic hydrogen*, Particle World **3** (1993) 139;
G. Fiorucci *et al.*, Nucl. Instr. and Meth. **A292** (1990) 141;
D. Varidel *et al.*, Nucl. Instr. and Meth. **A292** (1990) 147.

[7] EEV (English Electric Valve), Waterhouse Lane, Chelmsford, Essex, CM12QU, England.

[8] D. Sigg, Nucl. Instr. and Meth. **A345** (1994) 107.

[9] D. Anagnostopoulos *et al.*, Phys. of Atomic Nuclei **59** (1996) 1503.

[10] B. Lauss, *Kaskade und Transfer von Myonen in Wasserstoff*, Ph.D. Thesis, University of Vienna, 1997.

5 DAΦNE machine background

5.1 Sources of background from circulating beams

The DEAR experiment on DAΦNE is the first attempt to use CCDs in the vicinity of an e^+e^- collider. DAΦNE is a low energy e^+e^- collider (0.51 GeV per beam), with a designed luminosity of $5 \times 10^{32} cm^{-2} s^{-1}$ in the 120-bunch mode at a current of 5 A [1]. Due to the low energy and the high current, particles are lost from the machine at a high rate and could be a serious source of background.

The number of particles per bunch is 8.9×10^{10} and the estimated beam lifetime is on the order of two hours at the working pressure of 10^{-9} Torr (the residual gas is mainly diatomic oxygen), *thus the rate of loss of particles per bunch per beam over the whole ring is:*

$$R_{loss} = \frac{circulating\ particles}{beam\ lifetime} \simeq 12\ MHz/bunch/beam \tag{40}$$

This value must be multiplied by the factor $2 \times 120 = 240$ for the two beams at full luminosity.

In a low energy machine, the dominant cause of particle losses is *Touschek scattering* or elastic Coulomb scattering between two particles within the same bunch. The cross section σ is proportional to $1/\gamma^3$, with $\gamma = E/mc^2$. Touschek scattering results in a change of the longitudinal momentum of the two particles: one loses and the other gains the same fraction δ of momentum. If the change exceeds the acceptance of the ring, a particle is lost.

The second source of particle losses is the *beam-gas interaction.* The two main processes which characterize the interaction of the circulating beams of electrons and positrons with the residual gas in the machine pipe are Coulomb scattering and Bremsstrahlung on gas.

The rates of losses corresponding to these sources, deduced from different contributions to the single beam lifetime, are reported in Table 4. It is apparent that the Touschek effect is, by more than an order of magnitude, the greatest source of particle loss in DAΦNE. However, it is *not* the most relevant source of background in the interaction regions (IRs), since, unlike the beam-gas interaction, it can be almost entirely suppressed, as we shall see in the next Subsection.

Table 4: Rates of losses consistent with lifetime calculations.

Source	Contribution to lifetime	R_{loss}
Gas Bremsstrahlung	$2.0 \cdot 10^3$ min	0.74 MHz/bunch/beam
Coulomb gas scattering	$1.9 \cdot 10^3$ min	0.78 MHz/bunch/beam
Touschek scattering	160 min	9.2 MHz/bunch/beam
Single beam total lifetime	135 min	11 MHz/bunch/beam

Another possible source of background is synchrotron radiation. Radiation from upstream bending magnets does not reach the IRs, while that from the triplet of quadrupoles of the DAY-ONE IRs intercepts the beam pipe far downstream from the interaction point. That generated by the splitter magnets does not contribute to background in the interaction regions because the critical energy is only 29 eV [2] meaning that only 2.5×10^{-17} of the photons have an energy greater than 1 keV. Since the DEAR beam pipe is made of 600 μm carbon fiber and 250 μm aluminium, the number of photons with enough energy to escape from the beam pipe is so small that essentially no photons produced by synchrotron radiation emerge from the beam pipe.

Consider next those electrons and photons originating from e^+e^- annihilation:

- Bhabha scattering $e^+e^- \rightarrow e^+e^-$;
- radiative Bhabha scattering $e^+e^- \rightarrow e^+e^-\gamma$;
- two photon annihilation $e^+e^- \rightarrow \gamma\gamma$;
- beam-beam Bremsstrahlung.

These are created at the interaction point and are strongly forward scattered, thus few hit the beam pipe. Their contribution to background is orders of magnitude less than that of the main sources discussed above.

One must also consider "hadronic background" from ϕ decays to $\rho\pi$ (12.9 %) and to $\pi^+\pi^-\pi^0$ (2.4 %), as well as from the free decay of kaons to $\pi^\pm\pi^0$ (21.1%) and high energy photons from π^0s, either directly produced by K^-p absorption reactions, or as Λ and Σ^+ decay products.

The DEAR Monte Carlo, described in Section 6, evaluates both the kaonic hydrogen X-ray yield and the number of particles and X rays reaching the CCDs originating either from "machine background" or "hadronic background". The contribution, in terms of hits and of X rays, from the "hadronic background" is one order of magnitude smaller than that coming from "machine background".

5.2 Touschek scattering

In the DAΦNE rings, two regions can be distinguished: straight sections with vanishing dispersion, and arcs with high dispersion. Particles Touschek scattered in the straight sections undergo a momentum deviation δ, but no betatron oscillation and, therefore, cannot be lost in the IRs where the dispersion is zero. Particles scattered in the arcs gain a horizontal betatron oscillation and can, if lost on the walls of the vacuum chamber in the IRs, produce background in the detectors. However, all particles which undergo Touschek scattering follow similar trajectories, i.e., with the same betatron oscillation phase and an amplitude proportional to the momentum deviation δ. Since they are in the horizontal plane in a narrow cone of about 20 mrad, it is possible to reduce the background by:

- increasing the vacuum chamber aperture inside the detectors;

- inserting beam scrapers of 3.5 mm Tungsten - about 10 radiation lengths upstream of the splitter magnet of each interaction region, to remove the large amplitude particles.

The effect of these changes was also included in the Monte Carlo calculations [3,4].

In Figure 6 the DAΦNE general layout is shown. The two colliding beams run in two separated rings, which overlap in the interaction regions called KLOE IR and FINUDA IR. Each ring is made of an internal part (SHORT) and an external one (LONG).

The DEAR set-up will be installed during the initial stage of DAΦNE operation, in one of the interaction regions designed for machine commissioning (the so-called DAY-ONE IR), after removing the central quadrupole situated on the interaction point (IP) and inserting the DEAR beam pipe. Readjusting the strength of the remaining quadrupoles of the IR will match to the optics transparency condition of the ring.

Due to the horizontal crossing angle, the layout of the machine is not symmetric with respect to the interaction points. In the KLOE IR, the beams come from the external (LONG) ring and give rise to the first interaction in the machine. In the FINUDA IR, the beams come from the internal (SHORT) ring. The beams coming from the LONG ring have a better emittance with respect to the average machine value. As a consequence, the rate of particle losses, due to Touschek scattering, is higher in the FINUDA interaction region. With a suitable beam-scraper aperture, this background can be practically eliminated in the KLOE interaction region and strongly reduced in the FINUDA one, as shown in Table 5 [5]. The rates for positive and negative energy deviations are listed separately. Only particles with negative deviation constitute a significant source of background, because they are lost in the last quadrupole before the interaction point. Those with positive δ are lost in the quadrupole after the interaction point and have a small probability of becoming a source of background for DEAR.

5.3 Beam gas interaction

The simulation of the beam-gas interaction and the calculation of particle losses which create background has been performed using the TURTLE program (Trace Unlimited Rays Through Lumped Elements). It was created for the task of tracking charged particles through magnetic elements [6] and then adapted to include in-flight decay and, subsequently, to track both parent and daughter (neutral and/or charged) particles (DECAY_TURTLE) [7]. The current version includes beam-gas Bremsstrahlung, Coulomb scattering in gas and the electromagnetic showers produced in the slits along the beam line [8].

For the products of beam-gas interactions on nuclei of residual gas, the program takes into account the following two cross sections (and uses the proper kinematic distributions). The Coulomb scattering cross section for relativistic electrons is [9]:

$$\frac{d\sigma}{d\Omega} = \frac{4Z^2 r_e^2}{\gamma^2} \frac{1}{(\theta^2 + \theta_1^2)^2} \quad , \tag{41}$$

where:

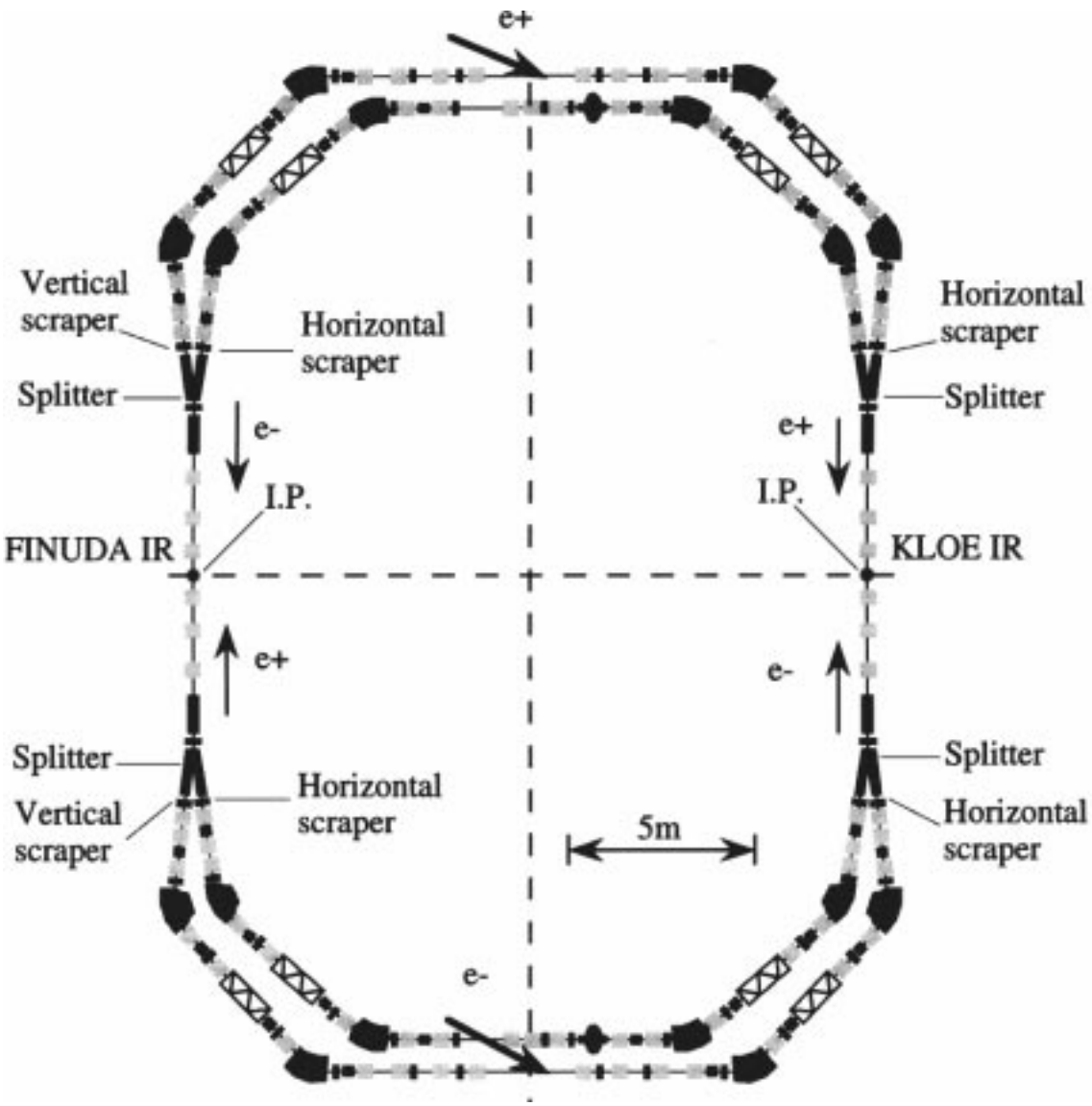

Figure 6: DAΦNE general layout with the DAY-ONE IRs in the DEAR configuration (i.e., without the central quadrupole). Scrapers and splitters are also indicated.

Table 5: Particles lost due to Touschek scattering in the DEAR interaction region (A_{SC} the scraper aperture; σ_x the horizontal beam size; τ_{tot} single beam lifetime).

A_{SC}/σ_x	A_{SC} (mm)	N_{DEAR} (KLOE IR) (s^{-1}/bunch/beam)			τ_{tot} (min)
		$\delta < 0$	$\delta > 0$	total	
no scrapers	43	$7.73 \cdot 10^5$	$6.03 \cdot 10^4$	$8.33 \cdot 10^5$	139
11	31	0	323	323	138
10	28	0	0	0	124

A_{SC}/σ_x	A_{SC} (mm)	N_{DEAR} (FINUDA IR) (s^{-1}/bunch/beam)			τ_{tot} (min)
		$\delta < 0$	$\delta > 0$	total	
no scrapers	43	$8.77 \cdot 10^4$	$1.10 \cdot 10^5$	$1.97 \cdot 10^5$	97
10	31	$7.45 \cdot 10^3$	$2.71 \cdot 10^4$	$3.46 \cdot 10^4$	96
9	28	725	$7.38 \cdot 10^3$	$8.11 \cdot 10^3$	90
8	25	35	$1.01 \cdot 10^3$	$1.05 \cdot 10^3$	77
7	22	0	55	55	63

$$\theta_1 = \alpha Z^{1/3} \frac{1}{\gamma} \ , \tag{42}$$

with Z the atomic number of the nuclei of residual gas, r_e the classical electron radius, γ the electron energy in units of rest mass and α the fine structure constant.

For beam-gas Bremsstrahlung [9]:

$$\frac{d\sigma}{dk} = \frac{1}{n_a X_0 k}[1 + (1-\nu)(1 - \nu + \frac{1}{9ln(183/Z^{1/3})} - \frac{2}{3})] \ , \tag{43}$$

where n_a is the number of atoms per unit volume at atmospheric pressure, $\nu = k/E_0$ is the energy of the emitted photon relative to the electron energy and the radiation length X_0 is given by the following expression, which takes into account both the scattering on the nucleus and that on the electrons of the residual gas atoms:

$$\frac{1}{X_0} = 4\alpha r_e^2 n_a Z(Z+1.3) ln \frac{183}{Z^{1/3}} \tag{44}$$

Coulomb scattering changes only the direction of the scattered electrons, not their energy. The ϕ (polar angle) deviation is chosen randomly by TURTLE. The θ (azimuth) distribution is weighted with the cross section.

Bremsstrahlung processes change only the momentum and not the direction of scattered electrons. The momentum variation is performed by using a random procedure weighted with the corresponding cross section.

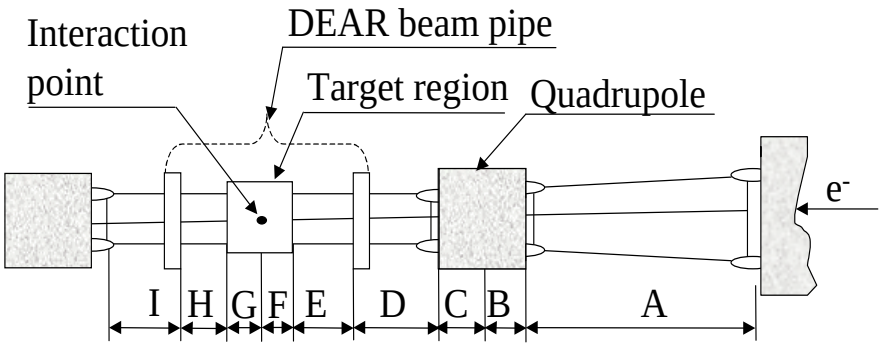

Figure 7: Sectors in the DAY-ONE DEAR IR considered in counting the lost particles.

Simulations were performed [10] for both IRs for one complete turn in the machine following the sense of one circulating beam, starting at the end of the splitter magnet "downstream" from an IR, and ending 0.45 m after the IP of that IR.

The region near the IP was devided into 9 sectors (see Figure 7). The resulting longitudinal distribution of the lost particles is the input for the DEAR Monte Carlo, which evaluates the number of particles reaching the CCD detector from each single sector.

Coulomb scattering (C.S.) was simulated for the angular interval from 1 mrad to 500 mrad. Bremsstrahlung simulation was performed for two ranges of momentum variation (the intervals were chosen taking into account the cross section variation):

Hard Bremsstrahlung (H.Br.) [Δp/p: $20\% - 90\%$]

Soft Bremsstrahlung (S.Br.) [Δp/p: $0.2\% - 20\%$]

The distribution of Bremsstrahlung particles is in the horizontal plane because the momentum variation produces a spread of amplitudes in the horizontal plane when the particles pass through the bending magnets. The Coulomb scattered particles are evenly distributed around the beam, because their momenta do not change in ϕ.

In Table 6 from ref. [10], particle losses in the different segments are listed for the case of the FINUDA interaction region, where the DEAR set up will be located. The rates are valid for a constant gas pressure of 10^{-9} torr.

Since the beams are entering the IRs from the LONG (KLOE) and SHORT (FINUDA) rings, respectively, the beam trajectory passes off axis in the quadrupoles of the IRs, and, therefore, the particles are lost mainly on one "side" of the pipe. This side changes from one IR to the other – the trajectories are shifted to the outside of the geometrical axis in the KLOE IR and to the inside in the FINUDA IR.

Table 6: Rates (in kHz) of lost particles (electrons, photons) per beam in sectors of the FINUDA IR, in the DEAR configuration.

Losses	A	B	C	D	E	F	G	H	I
C.S. e^-	53.7	11.3	8.8	4.7	15.3	6.4	9.1	45.6	21.9
H.Br. e^-	28.3	8.4	4.6	2.3	6.9	2.2	2.2	9.1	3.7
H.Br. γ	1.5	0.4	0.4	0.25	0.7	0.15	0.15	0.6	0.2
S.Br. e^-	107.	17.5	0	0	0	0	0	0.02	0.17
S.Br. γ	6.1	2.1	1.5	0.85	2.1	0.4	0.5	2.2	33.7

Table 7: Pressure-normalized rates (in kHz) of lost particles (electrons, photons) per beam in sectors of the FINUDA IR in the DEAR configuration.

Losses	A	B	C	D	E	F	G	H	I
C.S. e^-	41.3	8.7	6.1	3.57	10.9	3.78	5.9	31.5	16.2
H.Br. e^-	6.79	2.02	1.1	0.55	1.66	0.53	0.53	2.2	0.89
H.Br. γ	0.23	0.06	0.07	0.04	0.1	0.03	0.03	0.12	0.05
S.Br. e^-	37	6	0	0	0	0	0	0	0
S.Br. γ	0.97	0.34	0.26	0.15	0.40	0.18	0.10	0.46	9.1

The Coulomb scattered electrons are distributed in a region 20 m upstream of the IP, which corresponds to about one quarter of the ring. Although these electrons hit the pipe along the ring, many hit the scrapers.

The origins of the electrons which emit hard Bremsstrahlung and are lost near the interaction point are concentrated between the splitter and the IP because these electrons, having had a large momentum variation, are quickly lost after passing through a bending magnet.

To take into account the variation of the pressure along the DAΦNE rings, the rates of Table 6 must be multiplied by a corresponding pressure normalization factor, calculated by integrating the distribution of lost particles weighted with the local pressure.

Since the gas pressure in the straight sections, especially the IRs, is lower than 10^{-9} torr, all rates in Table 6 will be reduced. In particular, electrons lost by H.Br. originating in the IRs are strongly reduced and the contribution of the H.Br. photons becomes negligible. Electrons lost by S.Br. are significant only in sector A. Therefore, Coulomb scattering is the main contributor to particle losses due to beam-gas interactions. The pressure-normalized rates of particles are given in Table 7.

References

[1] G. Vignola, *DAΦNE: the first ϕ-Factory*, Proceedings of the *5th European Particle Accelerator Conference (EPAC'96)*, Sitges (Barcelona), Eds. S. Myres *et al.*, Institute of Physics Publishing, Bristol and Philadelphia, 1996, pag. 22.

[2] M. Sullivan, *Preliminary background calculations for DAΦNE*, DAΦNE Technical Note IR-2, 1993.

[3] S. Guiducci, *Background in the KLOE IR due to Touschek scattering*, DAΦNE Technical Note IR-5, 1994.

[4] S. Guiducci, *Background evaluation in DAΦNE*, DAΦNE Technical Note IR-6, 1995.

[5] S. Guiducci, *Background calculation for the DAΦNE experiments*, Proceedings of the *5th European Particle Accelerator Conference (EPAC'96)*, Sitges (Barcelona), Eds. S. Myres *et al.*, Institute of Physics Publishing, Bristol and Philadelphia, 1996, pag. 1365.

[6] D.C. Carey, *Report* NAL-64, Dec. 1971.

[7] K.L. Brown, D.C. Carey and Ch. Iselin, SLAC-246 UC-28 (1/A) 1982.

[8] W. Kozanecki and J. Matthews, TURTLE (TUR-107 A version) program manual, SLAC Library.

[9] B. Rossi, *High Energy Particles*, Prentice-Hall Inc., Englewood Cliff, N.J., 1952.

[10] S. Guiducci and M.A. Iliescu, *Beam-gas background calculation for DEAR*, Frascati Report LNF-97/002 (IR) (1997).

6 Expected rates and background

6.1 The DEAR Monte Carlo

A Monte Carlo calculation was performed in the framework of the CERN simulation package GEANT3 [1], using an improved version of the 3.21 code, to simulate the physical processes involved in a kaonic hydrogen experiment to optimize the geometry (dimensions, materials, etc.) and performance (counting rate, background contamination).

The program generates the primary ϕ mesons produced in e^+e^- collisions, taking into account the electron and positron energy spread and beam dimensions in the crossing point, according to the parameters expected for DAΦNE. The ϕ mesons are then allowed to decay to all relevant final states, according to known branching ratios.

Decay particles are followed through the experimental setup considering energy loss and multiple scattering. They are then allowed to decay or interact both electromagnetically (generating e.m. showers), and hadronically. The following hadronic interactions of a K^- with a proton at rest (in the gas target or frame) are switched on by an external routine:

$$\begin{aligned} K^- + p \rightarrow \quad & \Lambda + \pi^0 \quad (7.5\%) \\ \rightarrow \quad & \Sigma^+ + \pi^- \quad (19.6\%) \\ \rightarrow \quad & \Sigma^- + \pi^+ \quad (46.7\%) \\ \rightarrow \quad & \Sigma^0 + \pi^0 \quad (26.1\%) \end{aligned}$$

along with the corresponding channels for the K^-n interaction. Nuclear binding effects and final state interactions are considered. The resulting particles are allowed to decay or interact, eventually generating e.m. showers of electrons, positrons and photons. Tracking stops upon reaching a CCD.

Using the results of calculations described in Section 5, the e.m. showers resulting from high energy electrons and photons striking the beam pipe and the experimental setup are calculated. A record is kept of particle type, deposited energy, momentum and positions of particles hitting the CCDs.

Finally, an X ray of 6.5 keV is generated for each K^--stopping inside the hydrogen target to simulate the emission of X rays from the $2p \rightarrow 1s$ transition.

The reliability of the code depends critically on its performance at very low energies. In particular, the behaviour of photons, electrons and positrons must be accurate below the 10 keV low energy cut-off of the standard GEANT package.

It was verified that the GEANT program remains accurate below 10 keV for photon interactions, in particular for the photoelectric process, which is the relevant one for energies below 100 keV.

The Bremsstrahlung process is treated in the GEANT package by three different routines: GBRELE, GBRSGE and GBREME, which are all based on the Bremsstrahlung cross section values tabulated in ref. [2] for various materials and for electron energies from 1 keV up to 10 GeV. In all the routines, a fundamental role is played by the parameter

k_c, which is the low energy cut-off. k_c is the photon energy below which the Bremsstrahlung process is treated only as a continuous energy loss of the electron (positron) to be summed up to the ionization energy loss (routine GBRELE). Above k_c, the energy and angular distribution of the Bremsstrahlung process are treated by the routine GBREME. To calculate the total Bremsstrahlung cross section, the routine GBRSGE is used. It was verified that the values calculated by the routines GBRELE and GBREME are also accurate down to 1 keV.

However, the total cross section values calculated by the routine GBRSGE are unreliable when the cut-off parameter k_c is set below 10 keV: for example, the points corresponding to $k_c = 2\ keV$ show an unphysical peak for an electron energy around 100 MeV. Therefore, in order to recover the expected logarithmically increasing behaviour of the Bremsstrahlung cross section as a function of the electron energy T, the GBRSGE routine was modified for $k_c < 10\ keV$ so that:

$$\sigma_{Brem} = \alpha(k_c) + \beta(k_c)\log(T)\ \ , \tag{45}$$

where the values of the parameters $\alpha(k_c)$ and $\beta(k_c)$ were obtained from a fit of the cross section values above k_c = 10 keV. It was estimated that the error on this approximation is no worse than the 10-15% error quoted for the GEANT code between 10 keV and 1 MeV.

6.2 DEAR Monte Carlo results

The momentum distributions of the π^+, μ^+ , photons, etc., on reaching the CCD detectors are obtained through the Monte Carlo. An example is given in Figure 8, where the momentum distribution of positive pions is shown. The main physical features are well reproduced, showing that the additional routine to GEANT3 properly takes into account the K^--nucleon interaction at rest.

6.2.1 Signal rate

At the 30-bunch luminosity $L = 1.2 \cdot 10^{32}\ cm^{-2}\ s^{-1}$, the annihilation cross section of 4.4 μb at the ϕ-resonance produces a $K^{\pm}$ flux of 220 s^{-1} at a central momentum of 126.9 MeV/c, with a momentum spread $\delta p/p \simeq 10^{-3}$.

Using these results and the geometry described in Section 3, the Monte Carlo predicts:

- the number of K^- entering the target volume: $N_{in}^K = (12.5 \pm 0.2)$/s, corresponding to $(5.7 \pm 0.1)\ \%$ of the produced kaons;
- the number of K^- stopped in the hydrogen gas: $N_{st}^K = (8.6 \pm 0.1)$/s, corresponding to $(68.8 \pm 1.4)\ \%$ of the kaons entering the target.

The predicted number of K_α events with $\rho_H = 3.6 \times 10^{-3}\ g/cm^3$, $\epsilon_{CCD}(6.5\ keV) = 60\%$, $Y(2p \to 1s) = (1-3)\%$ is then:

$N(K_\alpha) = (7-21)$/hour.

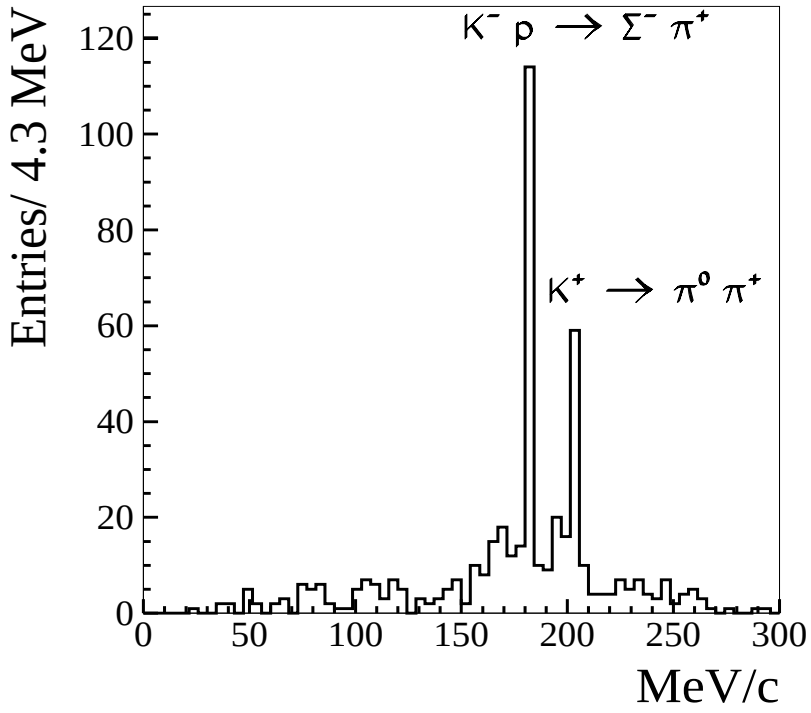

Figure 8: Momentum distribution of positive pions hitting the CCDs. The peak from the reaction $K^- p \to \Sigma^- \pi^+$ at 182 MeV/c and the peak from the decay $K^+ \to \pi^0 \pi^+$ at 205 MeV/c are clearly reproduced, together with their relative strength.

6.2.2 Background evaluation

The CCD background can be divided into two categories. The first is the background which affects the operational conditions of a CCD causing its "blindness" from "double hits" as explained in Section 4. This background is given directly by the number of ionizing particles which hit the surface of half a CCD between readout times. The second is the soft (below 10 keV) X-ray background in the energy region of the signal. This background cannot be eliminated, as the CCD is a non-triggerable detector.

The background particles have two sources: background generated by ϕ-decay products, among which an important role is played by the hadronic interaction of the stopped K^-. This has been defined as the "hadronic background". The second source is the "machine background", consisting of the products of the electromagnetic cascades generated by the electrons and positrons lost from the primary beams circulating in the rings. As discussed in Section 5, the beam losses are due to the Touschek effect and to beam-gas interactions (large angle Coulomb scattering and Bremsstrahlung on the residual gas).

Hadronic background

Particles coming from the ϕ-decay directly or as secondary products of hadronic interactions can directly hit the CCDs, depositing energy over several pixels thus contributing to the CCD "blindness". Photons coming from π^0 decay initiate electromagnetic showers, which can produce soft X rays which are "true" background. With 10^6 ϕs generated by the Monte Carlo program, corresponding to 38 minutes of beam time, 9510 ionizing hits on CCDs and 6 X rays below 10 keV were obtained.

This low hadronic X-ray background on CCDs can be explained by the 30μ m thickness of the depletion layer, which prevents electrons or positrons from radiating inside the CCDs. In contrast, the Si detectors used in the previous kaonic hydrogen experiments had a high hadronic background of soft X rays due to their thickness of a few mm (necessary in order to obtain a 100% detection efficiency), causing the detector itself to act as radiator for electrons and positrons. This is seen clearly from the Monte Carlo result shown in Figure 9. The figure reproduces the experimental behaviour of the energy deposition on a CCD from charged particles and characterizes the types of particles responsible for this deposition: among particles whose energy deposit is less than 50 keV, the presence of photons is negligible.

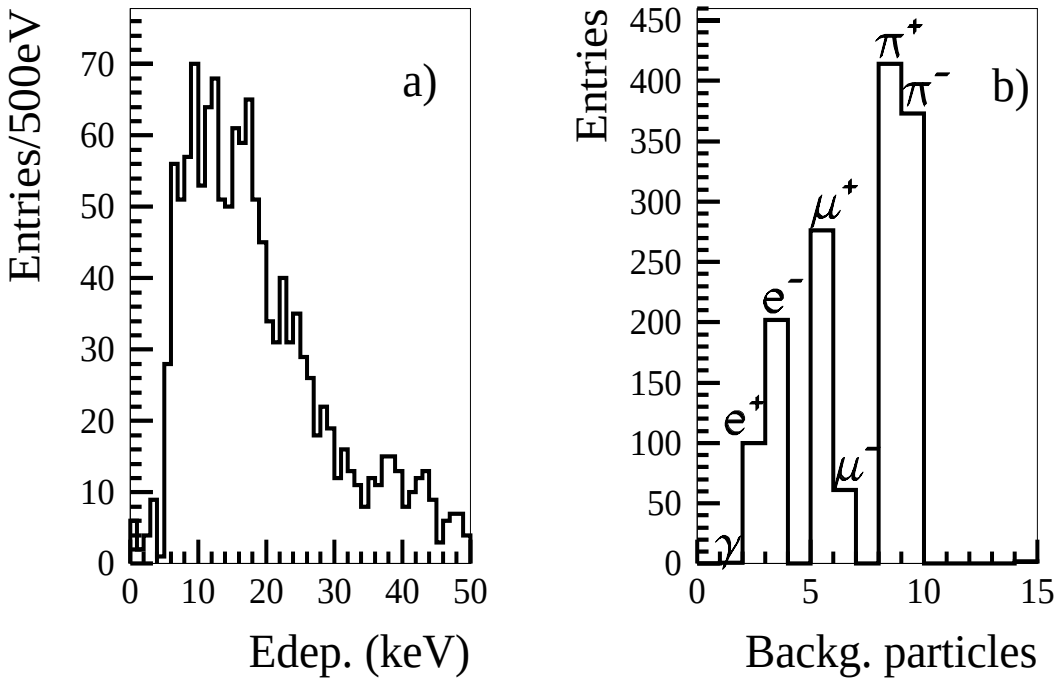

Figure 9: a) Energy deposition below 50 keV in the CCDs; b) types of particles whose energy deposition in CCDs is less than 50 keV.

Table 8: Summary of the DEAR Monte Carlo background results for the FINUDA IR in the DEAR configuration

Type of background	Hadronic	Touschek	Beam-gas	Total
Particles lost from 2 beams (kHz) in the DAY-ONE DEAR IR		43.5	546.6	590.1
Hits on 1/2 CCD (min^{-1})	16	108	475	599
X rays (h^{-1}) over 1 keV in the signal region	1.2	15.3	57.0	73.5

Background from Touschek effect

The background coming from the Touschek effect was studied using the DEAR Monte Carlo program. A few million electrons were generated which hit the pipe with the kinematics of particles lost by Touschek scattering. Their interaction with all the materials present in the experimental setup was considered and the showers, including particles created, were followed down to 1 keV and all particles hitting the CCDs were then recorded. Using an overall lost-particles rate at the 30-bunch luminosity of 43.5 kHz (Table 5 $A_{SC}/\sigma_x = 9, \delta < 0$) in the FINUDA interaction region, one obtains:

- Number of particles depositing energy = 0.81 particles/cm^2/s. This corresponds to 108 particles/min for half a CCD.

- Number of X rays/keV in the signal region = 15.3/hour

Background from the beam-gas interaction

The overall rates of lost particles due to beam-gas interaction, reported in ref. [3] and briefly presented in Section 5, were used as input to the DEAR Monte Carlo. Tens of millions of electrons were generated taking into account the kinematics and rate for each sector considered for the FINUDA IR in the DEAR configuration (see Section 5).

Table 8 summarizes the Monte Carlo results for background coming from the three main sources: hadronic, Touschek effect and beam gas interaction. The global number of hits on half a CCD (which determines the readout time) and the X-ray background on the 8 CCD detectors are presented separately.

Table 9: Summary of the DEAR Monte Carlo background results using shielding

Type of background	Hadronic	Touschek	Beam-gas	Total
Particles lost from 2 beams (kHz) in the DAY-ONE DEAR IR		43.5	546.6	590.1
Hits on 1/2 CCD (min^{-1})	16	11	48	75
X rays backgr. (h^{-1}) over 1 keV in the signal region	1.2	1.3	10.5	13.0

6.2.3 Background suppression by shielding

With a signal of 7-21 counts/hour spread over 1 keV, the signal-to-background ratio ranges from 1:10.5 to 1:3.5 over a spread of about 1 keV.

To perform a precision measurement, this background has to be reduced by shielding. With the help of DEAR Monte Carlo simulation, different shielding configurations were studied, and it was shown that a reduction of the X-ray background by up to a factor of 6 is possible. This reduction was achieved by using the following configuration:

- 2 lead walls, 20 cm thick, 1.5 m height, placed before the quadrupoles which are situated at the beginning and at the end of the interaction region;
- a 5 cm thick layer of lead placed on the DEAR platform, around the DEAR setup;
- a 5 cm thick layer of lead placed around the target vacuum jacket, in spaces left free;
- a 3 cm thick lead ring, with inner radius of 3.5 cm and outer radius of 15 cm, placed inside the DEAR platform hole, towards the setup, which allows the kaons to pass through to the target but stopping most background particles from reaching the setup.

With this shielding configuration, the Monte Carlo results for the FINUDA IR, on the CCD blindness and the X-ray background are reported in Table 9.

6.2.4 Summary

By using adequate shielding, the X-ray background can be reduced by a factor of 6. The signal-to-background ratio in this case ranges from 1:1.9 to 1:0.6, and would permit a measurement with a precision of about one percent. Moreover, the blindness level (about

75 particles/ 1/2 CCD /minute) does not create a read-out problem; a readout every 10 minutes being more than safe.

References

[1] R. Brun *et al.*, GEANT3, CERN Report DD/EE/84-1 (1987).

[2] M. Seltzer and M.J. Berger, Nucl. Instr. and Meth. **B12** (1985) 95.

[3] S. Guiducci and M.A. Iliescu, *Beam-gas background calculation for DEAR*, Frascati Report LNF-97/002 (IR) (1997).

7 Global precision of the measurement

The DEAR experiment has the capability to perform a measurement of the strong interaction shift and width of the K_α line of kaonic hydrogen to a precision of a few percent – a significantly greater precision than the KEK measurement [1] which reported a shift ranging between 250 and 400 eV. The precision is determined by the statistical error and many possible sources of systematic error. For a given number of X-ray events, the statistical error depends on the ratio of peak to background. Sources of systematic errors are:

1. uncertainty in the calculation of the position of the unperturbed (purely electromagnetic) K_α line;
2. non-linearity of the X-ray CCD detectors;
3. energy calibration of the X-ray CCD detectors;
4. uncertainty in the fitting procedure.

7.1 Sources of systematic error

The following analysis of the sources of systematic error in the DEAR experiment is based on the content of ref. [2].

7.1.1 Electromagnetic transition energies

To measure the strong interaction component of the kaon-nucleon interaction at low energy, one measures the shift ϵ of the position of the K_α line from that calculated on the basis of a purely electromagnetic interaction. This may be expressed as:

$$\epsilon = E_{2p\rightarrow 1s}^{measured} - E_{2p\rightarrow 1s}^{e.m.} \tag{46}$$

The electromagnetic $2p \rightarrow 1s$ transition energy in kaonic hydrogen is calculated by solving the corresponding Klein-Gordon equation and then applying corrections for finite size and QED effects, especially vacuum polarization. The value of the transition energy so obtained is $6480 \pm$ 1 eV [1], where the error is dominated by the uncertainty of the kaon mass. This 1 eV error directly contributes to the uncertainty of ϵ.

7.1.2 Linearity of the CCD detectors

Based on the physical processes leading to charge deposition in the CCD material, the response must be linear. However, the response of the detection system as a whole, including amplifiers and ADCs, must be determined experimentally.

The chips and their corresponding readout electronics packages (so-called Readout Boxes) were exposed to X-ray sources of multi-material targets which were activated by a

strong radioactive source. The resulting spectra were fit [3] with multi-Gaussian peaks to yield the mean channel of each calibration peak. A plot of the fit channel versus the known energies of the fluorescence X rays was fitted to both a linear and a quadratic function. The χ^2 of a quadratic fit was found to be the same as that for a linear fit, indicating that the quadratic term was consistent with zero (see Figure 10). For an estimate of the systematic uncertainty, the error on the quadratic term was taken. This implied an upper limit on the error in the region of the kaonic hydrogen K_α peak of the order of 2 eV.

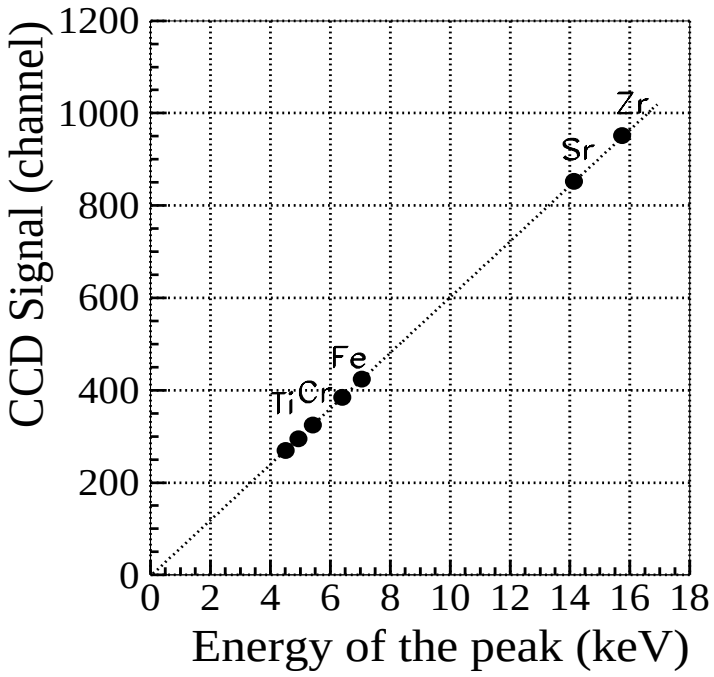

Figure 10: Linearity of the CCD signal versus energy using multi-material targets excited by a strong radioactive source.

7.1.3 Energy calibration of the CCD detectors

Given the results of the linearity calibration discussed above, one might be tempted to use these results to determine the energy corresponding to the mean channel of the K_α peak. The energy scale of a given detector can change over long periods of time due to temperature, radiation, or other unknown effects. Thus a so-called *long-term calibration scheme* has been implemented to partially eliminate this problem. The walls of the cryogenic target have been lined with titanium and zirconium foils. Electronic X rays will be excited in these foils by kaons, pions, and other high-energy beam-related background

particles, and these X rays will be measured simultaneously with the kaonic hydrogen X rays. Thus the final fit of the kaonic hydrogen spectra will automatically include the precisely-known peaks from titanium and zirconium. Small random shifts in the detector gain will be convoluted with the natural Gaussian width of the detector response function, and will be measured and included in the fit of these *long-term calibration peaks*, which in turn will be used to determine the energy of the mean channel of the kaonic hydrogen K_α peak.

However, this is not a complete solution. It could happen, for example in the case of a steady gain degradation over the course of the experiment, that the additional width introduced by the gain shift is large compared to the detector resolution, leading to badly degraded statistical performance. Even more dangerous would be sudden large jumps in the gain of a detector, which would lead to convoluted multiple peaks in the final spectra.

This latter effect was seen during long-term CCD stability tests. These tests were performed using a ^{55}Fe source (Mn K_α= 5.9 keV) irradiating 4 CCDs, and in general indicated a fluctuation of the peak position of about 20 eV (FWHM) over a period of one month. Some unexplained systematic jumps were also observed.

In order to guard against these potential problems, a so-called *periodic stability check* will also be implemented. This will involve ten to fifteen minutes of data-taking per day, during which kaonic X rays will not be measured, but rather fluorescence X rays from Ti calibration foils, excited by a strong radiation source inserted between the target entrance window and the insulation vacuum entrance window. Test measurements indicate that about 3000 counts/hour/ 1/2 CCD can be induced with a 17-MBq ^{55}Fe source. Monte Carlo studies show [4] that just a few hundred counts per peak are enough to track any shifts larger than 20 eV. Using data from the stability check, the daily accumulated spectra can be scaled appropriately before being added to the final spectra.

By implementing the long-term calibration scheme and periodic stability checks as described, it will be possible to compensate for any sudden systematic gain shifts, which could severely compromise the ability to fit the final kaonic hydrogen spectra. Instead, a set of well-behaved spectra with the narrowest possible calibration peaks from titanium and zirconium built-in will become available. In this case, the main systematic error in the energy calibration of the kaonic hydrogen K_α peak will be determined by the precision to which the positions of the calibration peaks are known, which is in turn a question of statistics.

An estimate was made based on the flux of low energy photons (below 100 keV) in the DEAR target, using the DEAR Monte Carlo program. This study was combined with a simulation to determine the spatial arrangement of the calibration foils within the target, which would give an error in the peak position determination at 6.5 keV of the order of 1 eV.

The simulation was based on the results of laboratory tests [5] regarding the relative intensities of titanium and zirconium K_α X rays, for identical configurations (same area and position) and under the same excitation source, in this case the X-ray line at 18.611 keV of an ^{241}Am source.

Assuming a yield of 1 (3)% of the $2p \rightarrow 1s$ transition, the Monte Carlo results show

that one can expect 4.5 (1.5) Ti K_α X rays along with 1 kaonic hydrogen K_α X ray and, in addition, 3 (1) Zr K_α X ray in the final kaonic hydrogen spectrum. With 15000 Ti events and 10000 Zr events, the energy of the mean channel of the fit kaonic hydrogen K_α can be determined to within 1.0 eV.

The energies of the electronic X rays of the two calibration peaks are known to within 0.05 eV [6]. This has a negligible effect included in the systematic uncertainty in the energy scale calibration. Assuming that the projected ratios of calibration X rays to kaonic hydrogen X rays are correct, the systematic error associated with the CCD energy scale will always be smaller than the statistical error.

7.1.4 Uncertainty in the fitting procedure

Extensive Monte Carlo studies of the fitting procedure for the final kaonic hydrogen spectra were performed. It was demonstrated that it is possible to fit multiple kaonic hydrogen peaks and calibration peaks over a large but smooth background without introducing any systematic biases. However, in order to achieve these unbiased fits, three important pieces of information are required: the efficiency of the CCDs as a function of energy, the energy resolution of the CCDs as a function of energy, and the background shape.

The CCD efficiency has been successfully modelled and measured, including the effects of window absorption [7]. Monte Carlo studies indicate that the present level of uncertainty in the efficiency will not introduce any significant systematic bias in the fit of the final spectra.

The CCD energy resolution as a function of energy is well-modelled by Eq. (38). Measurements of the factor N were obtained as a bonus when the linearity characterization for each detector was performed - the fit peak widths were plotted as a function of energy and N was extracted from a fit of Eq. (38). The noise factor N is 15 electrons, with an error of the order of 5%.

To estimate the influence of this error on the fit width of the peak, two extreme cases have been considered. The optimal case is when N is known exactly; that is, it is a fixed parameter in the fit. In this case, the mean error on the fit width is 5 eV. The other extreme case allows N to be a free fit parameter, which increases the error on the K_α width from 5 to 10 eV. These comparisons indicate that the 5% uncertainty in N will have a negligible effect on the error of the peak fit width, and also showed that this uncertainty has no effect on the fit peak position.

One additional source of uncertainty related to the energy resolution is the fact that each fit peak is assumed to be a Gaussian (in the case of calibration peaks) or Voigtian (a convolution of a Gaussian with a Lorentzian, in the case of kaonic hydrogen peaks). These functions are defined only for a constant Gaussian width (σ) over the range of the peaks, which is not the case in a real detector. However, simulations have shown that making the approximation that the energy resolution is constant over the range of a given peak does not introduce any measurable systematic bias.

The final source of systematic error is the lack of knowledge concerning the background shape. There will certainly be a flux of real X rays illuminating the CCD detectors

with an energy distribution that can only be very roughly estimated. The rate of these X rays is estimated to be on the same order as that of the kaonic hydrogen X rays (see Section 6). This means that to measure the background directly (a lower limit) using an empty target would take an appreciable fraction of the running time and is not feasible. However, a partial measurement of the background under the kaonic hydrogen complex will be made automatically during a kaonic deuterium run.

If we assume the background under the peak to be smooth but not well-known (by making a linear fit to a quadratic background shape, for example), Monte Carlo studies show a small bias of the order of 1 eV on the fit peak position, but a large bias of the order of 15 eV in the fit peak width.

On the other hand, it is possible that the background would not be smooth if it contained X-ray peaks from contamination sources. For example, K_α X rays from iron at 6.4 keV would give a particularly dangerous background in a position that could be masked by the kaonic K_α peak and are sufficiently close in energy to introduce a significant shift-bias with relatively few events. Of course, the greatest possible care has been taken to exclude iron (and the equally dangerous manganese, K_α = 5.9 keV) from the DEAR target environment. The target cell itself was machined from a special low Manganese content ($\leq 0.15\%$) alloy of aluminium (AlMgSi 0.5), and is, in turn, more than 50% covered by titanium foils as part of the calibration scheme discussed above. The target vacuum chamber is made of the same alloy. All screws are either titanium or are titanium-coated. Thus, to first order there is no iron, manganese, or chromium within the solid-angle of the CCD detectors.

To quantify the effect of contamination peaks, a small (0.2% of the kaonic hydrogen peak) manganese peak that is entirely uncompensated (i.e., not fit) by the Monte Carlo was simulated. Such a peak would bias the fits and lead to a systematic shift in ϵ of less than 1 eV.

It should be mentioned that a *known* peak under the kaonic hydrogen K_α peak can be effectively fit without introducing any systematic biases. However, the necessary inclusion of additional free parameters to the fit would increase the statistical error of the fit.

Summary and estimate of the total systematic error

The estimated contributions to the systematic error on the strong interaction shift are summarized in Table 10. The expected systematic error in the measurement is 2.7 eV. When this is combined with the uncertainty in the calculated electromagnetic value, the measured systematic error of the shift of the K_α line in kaonic hydrogen is 2.9 eV, giving a relative error of slightly less than 1%, depending on the value of the shift.

7.2 Statistical error

Extensive Monte Carlo studies have been made to estimate the statistical errors on the shift and width under a variety of background and luminosity assumptions. A given Monte Carlo spectrum consisted of a linear background, two monoenergetic calibration

Table 10: Total systematic error

Source		**Error (eV)**
$E^{e.m.}_{2p\to 1s}$	theory	1.0
Detector Linearity		≤ 2.0
Energy Calibration	gain instability	negligible
	scale determination	≤ 1.0
	calibration energies	negligible
Fit Procedure	efficiency	negligible
	energy resolution	negligible
	constant σ assumption	negligible
	background shape	≤ 1.5
		≤ 2.7
	TOTAL:	*$\leq$ 2.9*

peaks (K_α and K_β of titanium), and five Lorentzian peaks from the kaonic hydrogen K-series (K_α through K_ϵ), all of which were convoluted with the energy dependent detector resolution and efficiency.

The values of the strong interaction shift and width, taken from the KpX analysis [1] were 323 eV and 407 eV, respectively. The relative intensities of the kaonic hydrogen K-series were also taken from fits of the KpX data [8] constrained by the cascade code of Borie and Leon [9]. The DEAR target will operate under similar conditions of temperature and pressure, and, as the uncertainty on the cascade calculations yielding these intensity ratios is fairly high, we consider this to be the most reasonable starting assumption.

To fit the generated spectra, a function S of the following form was used:

$$S = \sum_{i=0}^{p} B_i \cdot E^i + \sum_{k=1}^{m} C_k \cdot G(E_k^{cal}, \sigma(E)) + \sum_{j=1}^{n} A_j \cdot V(E_j^{em} + \epsilon, \sigma(E)\Gamma) \ , \qquad (47)$$

where E is energy, G is a Gaussian function, and V is a Voigtian function. The value E_j^{em} is the QED prediction of the purely electromagnetic transition energy of the jth K-series transition in kaonic hydrogen. These values are constants rather than parameters of the fit. Similarly, the energy-dependent energy resolution $\sigma(E)$ is also a pre-determined function and not a parameter of the fit. In the cases reported here, the background was fit with two

free parameters (p = 1), B_0 and B_1. There were two calibration peaks (m = 2), for an additional four parameters, the normalizations C_1 and C_2 and the positions E_1^{cal} and E_2^{cal}. Each of the five (n = 5) K-series peaks has a free normalization parameter, A_1 through A_5. Note however that the shift ϵ and width Γ are common to all kaonic hydrogen peaks, which adds only two additional free parameters to the fits, for a total of thirteen.

This function was convoluted with the detector response function and integrated over the spectral channel width of 100 eV.

An example of a generated spectrum and the resulting fit is shown in Figure 11. The χ^2 per degree of freedom of the fit is 1.07.

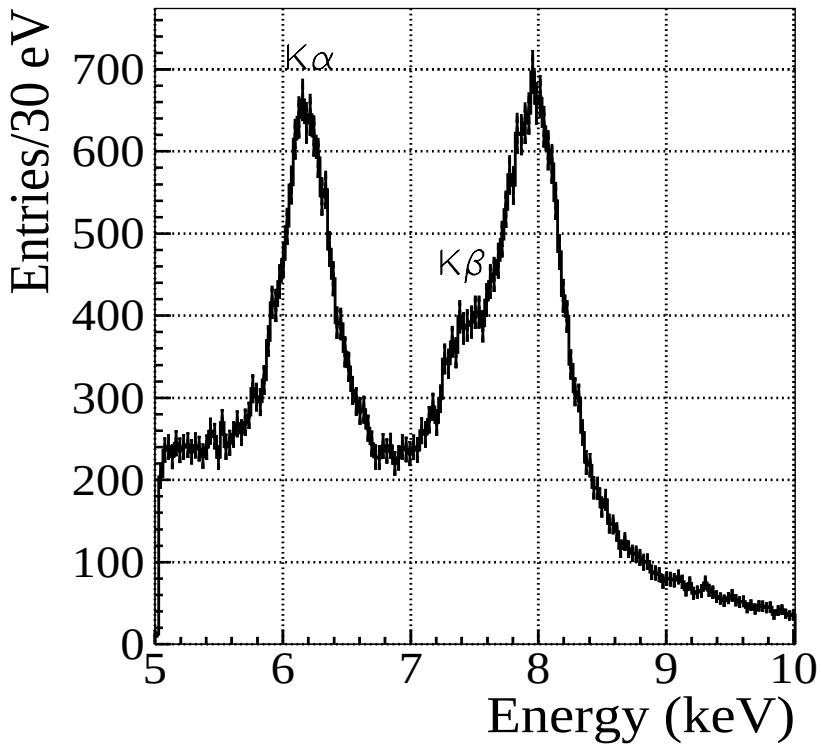

Figure 11: The K-complex pattern in kaonic hydrogen as generated by the DEAR Monte Carlo simulation for 10000 events in the K_α peak and a 60% background percentage.

To quantify the background, we refer to the background percentage (BG):

$$BG(\%) = \frac{\int_{-\Gamma/2}^{+\Gamma/2} B}{\int_{-\Gamma/2}^{+\Gamma/2} B + S} \times 100 \ , \tag{48}$$

where B is the background and S is the K_α signal, both of which are integrated over one Lorentzian width Γ of the kaonic hydrogen K_α peak.

The signal-to-noise ratio (S/N) over this region is related to the background percentage in the following manner:

$$\mathrm{S/N} = \frac{100}{\mathrm{BG}(\%)} - 1 \ . \tag{49}$$

For a given assumption of background percentage and luminosity, 1000 X-ray spectra were generated and fitted. For a given fit parameter, the width of the distribution of fit values was taken as an estimate of the statistical error on that parameter. A summary is listed in Table 11.

Table 11: Statistical precision

K_α events	Background (%)	$\Delta\epsilon$ (eV)	$\Delta\Gamma_{1s}$ (eV)
10000	0	3.5	5.9
	30	4.3	9.0
	60	6.2	13.7
	80	8.3	21.8
	90	12.6	28.0
5000	0	4.5	7.0
	30	6.1	14.5
	60	8.1	20.5
	80	11.6	30.8
	90	16.6	44.9
2000	0	7.2	11.1
	30	9.4	22.5
	60	12.8	32.7
	80	18.4	48.2
	90	25.7	68.5

From the table we note that, to reach a statistical precision on the position of the K_α line commensurate with a systematic error of a few eV, about 10000 events must be collected with a background better than about of 50% (signal to noise ratio 1:1). For a $2p \rightarrow 1s$ yield of 1 (3) % , the first condition is met with an integrated luminosity of 540 (180) pb^{-1} if the event rate is 7 (21) events per hour. A background of the level of 50%, can be obtained by shielding both within the interaction region and appropriately around the whole experimental setup, as described in Section 6. Thus, the results of our simulations show that the 1% goal is indeed obtainable within reasonably optimistic estimates of the event rate and background levels.

References

[1] M. Iwasaki *et al.*, Phys. Rev. Lett. **78** (1997) 3067.

[2] R. King, *"Statistical and systematic errors in the DEAR experiment"*, DEAR Technical Note IR-3, 1998.

[3] R. King and C. Petrascu, *"Linearity test of DEAR CCDs"*, DEAR Technical Note IR-4, 1998.

[4] T.M. Ito, *"Periodic stability check in DEAR"*, DEAR Technical Note IR-1, 1997.

[5] T.M. Ito and R. King, *"Summary of foil measurements, foil Monte Carlo, and recommendations for the long term calibration"*, DEAR Technical Note IR-2, 1998.

[6] J.A. Bearden, Rev. Mod. Phys. **39** (1967) 78;
J.A. Bearden and A.F. Burr, Rev. Mod. Phys. **39** (1967) 125.

[7] B. Lauss, *"Kaskade und Transfer von Myonen in Wasserstoff"*, Ph. D. Thesis, University of Vienna, 1997.

[8] T.M. Ito, *"Observation of Kaonic Hydrogen Atom X Rays"*, Ph. D. Thesis, University of Tokyo, UTPN-227, 1997.

[9] E. Borie and M. Leon, Phys. Rev. **A21** (1980) 1460.

8 Conclusions and perspectives

8.1 The DAΦNE ϕ-factory

DAΦNE has *unique features as a kaon source*, which should permit continuation of some projects already planned for aborted machines such as KAON at TRIUMF, or the European Hadron Facility.

The kaon beam is intrinsically clean, a situation *unattainable* with a *fixed target machine*. There, the minimum beam momentum is limited by the distance from the experiment to the production target and by the consequences of kaon decay in flight. The several hundred MeV/c momentum beams require the use of moderators, thereby enhancing the beam contamination at the experiment.

Also the machine environment is relatively clean or better under control. The sources of background (particles lost from the circulating beams due to Touschek scattering and beam-gas interaction, which make showers in the machine pipe and in the frame of the experimental setup) can be suppressed by adopting suitable shielding both *inside* the pipe (scrapers) and *around* the hot regions along the machine (lead walls) and, finally, by properly shielding the setup itself.

8.2 The DEAR experiment

DEAR has unique features for the observation of kaonic atoms. First, with a suitable choice of the gas density, the number of kaonic hydrogen K_α events collected in *one week*, at a $10^{32} cm^{-2} s^{-1}$ luminosity will exceed the present world data set by an order of magnitude.

The significant advantage of DEAR is the X-ray detector. First, CCDs have an intrinsic resolution three times better than that of any Silicon device used up to now in kaonic hydrogen measurements. Second, CCDs have an *unprecedented background rejection capability* – orders of magnitude better than that of a triggerable detector – due to the topology of energy deposition of a 6 keV X ray with respect to any ionizing particle. Low energy X rays deposit energy in *one pixel* only, whereas a particle (electron, pion, proton, neutron) deposits its energy over 5 pixels, on average, and can, therefore, be easily recognized and removed from the data sample.

A precision measurement - of the order of 1% - of the K_α line shift in kaonic hydrogen and a similar measurement on kaonic deuterium is significant for several reasons, as will be pointed out in the following three subsections.

8.2.1 Low-energy kaon-nucleon interaction

The first goal of DEAR is to study the low energy $\bar{K}N$ interaction, a field in which for nearly a quarter of a century no significant progress was made until the recent KpX experiment at KEK [1] which cleared up the discrepancy between scattering data and kaonic X-ray data.

Confirmation of this result with a precision measurement of the *repulsive* shift of the hydrogen K_α line, is theoretically significant. More significant, however, will be the first measurement of kaonic deuterium. Unlike the pionic atom case, the measurement of kaonic deuterium is required to determine the two isospin-dependent kaon-nucleon scattering lengths.

Measurements of the K_α series line shifts in kaonic hydrogen and deuterium will yield the $\bar{K}N$ scattering lengths a_0 and a_1 with a far better precision. This will drastically change the present status of low energy $\bar{K}N$ phenomenology.

8.2.2 KN sigma terms

Another consequence of the DEAR experiment is that one will be able to improve the determination of a vital quantity in non-perturbative QCD - the KN sigma term, which describes the degree of chiral symmetry breaking. In the SU(3) prescription, the KN sigma term is more strongly correlated with the strangeness content of the proton than is the πN sigma term, as emphasized by R.L. Jaffe and C.L. Korpa [2]. Only *estimates* of the KN sigma terms exist so far, due to poor KN scattering data at low energies, the phenomenological procedure, and unsettled issues in the chiral perturbation theory procedure. The issues in the latter procedure include the decuplet contributions and the convergence question associated with the renormalization schemes.

Phenomenologically, the KN sigma terms are determined from KN data by means of dispersion relations and by a continuation of the scattering amplitudes from the physical to the unphysical region. A 1% DEAR measurement at threshold would give a strong constraint to the bulk of low energy $\bar{K}N$ data, thus enabling the determination of the KN sigma terms more reliably, with an uncertainty significantly better than in the previous work - perhaps the order of 20%. According to Jaffe and Korpa, the determination of the strangeness content of the proton will also be much improved.

8.2.3 $\Lambda(1405)$ and sub-threshold $\bar{K}N$ interactions

The mass and width of $\Lambda(1405)$ have been determined relatively well through the $\Sigma\pi$ decay channel [3]. The $\bar{K}N$ interaction below the threshold is known less accurately than the Λ parameters themselves. Also, the question of the nature of $\Lambda(1405)$ is not yet resolved.

No quark model has yet placed $\Lambda(1405)$ properly in the SU(3) baryons mass scheme, while other baryon masses are calculated to be in a good agreement with observation. This puzzle continues to raise the question of what the $\Lambda(1405)$ really is: whether it is a Castillejo-Dalitz-Dyson (CDD) pole, a $\bar{K}N$ bound state, a resonance, an elementary three-quark state, a multiquark state, or an admixture of a $\bar{K}N$ bound state and a three-quark state.

The precise $\bar{K}N$ scattering lengths obtained from the DEAR data will substantially improve the knowledge of the sub-threshold $\bar{K}N$ dynamics and contribute to clarify the nature of $\Lambda(1405)$.

8.3 Perspectives: kaonic helium

Early experimental work on kaonic ^{4}He, done in the 1960's at the Argonne ZGS [4] and later at the Berkeley bevatron [5], resulted in spectra from a liquid helium target which showed clearly the L-series X rays at 6 to 9 keV but showed no evidence of the K-series. Physics of the kaonic helium interaction is more complex than for the hydrogen isotopes, and has several open questions. The essential aspect of the problem is understanding *how the* $\Lambda(1405)$ *behaves in the bound states of several nucleons.*

Although more recent measurements have been attempted, no data yet exist for ^{3}He. For ^{4}He, the L-series lines L_α, L_β and L_γ are at energies of 6.429, 8.867, 9.731 keV, and the K-series in both ^{3}He and ^{4}He is expected at the order of 30 keV, where the efficiency of our CCD is low. This implies to use a detector which is optimized in such energy range. Both the shift and width of the $2p$ and $1s$ levels in ^{3}He and ^{4}He are of interest. Presently, quantitative data exist only on transitions to the $2p$ level in ^{4}He [6]:

$$\epsilon \;=\; -35 \pm 12\; eV \qquad\qquad \Gamma \;=\; 30 \pm 30\; eV\;. \tag{50}$$

Theoretical predictions using a density dependent potential [7] strongly disagree with the data giving:

$$\epsilon \;=\; -0.4\; eV \qquad\qquad \Gamma \;=\; 1.3 - 1.6\; eV\;. \tag{51}$$

The calculated width of about 2 eV suggests that all kaons will be absorbed. The measured value disagrees with theory and would result in even stronger absorption in the $2p$ level. Thus only higher K-series X rays should be seen. This anomaly is unexplained.

No conclusive experimental data exist for either ^{3}He or ^{4}He on the $2p \rightarrow 1s$ transition. In this case, the density dependent potential shows [6] large differences between the two isotopes, both for shifts and for widths, while traditional theoretical approaches give roughly constant results. Both the shift and the width are predicted to be large - of the order of 6-8 keV, thus the measurements would be difficult.

References

[1] M. Iwasaki *et al.*, Phys. Rev. Lett. **78** (1997) 3067.

[2] R.L. Jaffe and C.L. Korpa, Comments Nucl. Part. Phys. **17** (1987) 163.

[3] R.H. Dalitz and A. Deloff, J. Phys. **G17** (1991) 289; (E) **G19** (1993) 1423.

[4] G.R. Burleson *et al.*, Phys. Rev. Lett. **15** (1965) 70;
S. Berezin *et al.*, Phys. Lett. **B30** (1969) 27.

[5] C.E. Wiegand and R.H. Pehl, Phys. Rev. Lett. **27** (1971) 1410.

[6] C. Batty, Nucl. Phys. **A326** (1979) 455;
S. Baird *et al.*, Nucl. Phys. **A392** (1983) 297.

[7] E. Friedmann, private communication.

Acknowledgements

We would like to thank the Swiss National Science Foundation for the support given to this work. We also thank the workshop of the Paul Sherrer Institute for the help is realizing the beam pipe for the experiment.

List of Figures

List of Tables